*J. Fluid Mech.* (2013), *vol.* 730, *pp.* 626–658.  
doi:10.1017/jfm.2013.356

# Effect of hinged leaflets on vortex pair generation

**Prashant Das, R. N. Govardhan† and J. H. Arakeri**

Department of Mechanical Engineering, Indian Institute of Science, Bangalore, 560012, India

(Received 4 October 2012; revised 11 April 2013; accepted 9 July 2013;
first published online 2 August 2013)

We experimentally study the effect of having hinged leaflets at the jet exit on the formation of a two-dimensional counter-rotating vortex pair. A piston–cylinder mechanism is used to generate a starting jet from a high-aspect-ratio channel into a quiescent medium. For a rigid exit, with no leaflets at the channel exit, the measurements at a central plane show that the trailing jet in the present case is never detached from the vortex pair, and keeps feeding into the latter, unlike in the axisymmetric case. Passive flexibility is introduced in the form of rigid leaflets or flaps that are hinged at the exit of the channel, with the flaps initially parallel to the channel walls. The experimental arrangement closely approximates the limiting case of a free-to-rotate rigid flap with negligible structural stiffness, damping and flap inertia, as these limiting structural properties permit the largest flap openings. Using this arrangement, we start the flow and measure the flap kinematics and the vorticity fields for different flap lengths and piston velocity programs. The typical motion of the flaps involves a rapid opening and a subsequent more gradual return to its initial position, both of which occur when the piston is still moving. The initial opening of the flaps can be attributed to an excess pressure that develops in the channel when the flow starts, due to the acceleration that has to be imparted to the fluid slug between the flaps. In the case with flaps, two additional pairs of vortices are formed because of the motion of the flaps, leading to the ejection of a total of up to three vortex pairs from the hinged exit. The flaps' length ($L_f$) is found to significantly affect flap motions when plotted using the conventional time scale $L/d$, where $L$ is the piston stroke and $d$ is the channel width. However, with a newly defined time scale based on the flap length ($L/L_f$), we find a good collapse of all the measured flap motions irrespective of flap length and piston velocity for an impulsively started piston motion. The maximum opening angle in all these impulsive velocity program cases, irrespective of the flap length, is found to be close to 15°. Even though the flap kinematics collapses well with $L/L_f$, there are differences in the distribution of the ejected vorticity even for the same $L/L_f$. Such a redistribution of vorticity can lead to important changes in the overall properties of the flow, and it gives us a better understanding of the importance of exit flexibility in such flows.

**Key words:** jets, propulsion, vortex flows

† Email address for correspondence: raghu@mecheng.iisc.ernet.in

## 1. Introduction

An unsteady starting jet is a frequently observed phenomenon in natural biological systems, which has found application in various applied engineering problems. These have been associated with various propulsive systems, both in the ocean and in aviation. To give an example, aquatic animals such as squids and jellyfish rely on a series of unsteady starting jets to propel themselves (Anderson & Demont 2000; Dabiri *et al.* 2005). Starting jets are also observed in the discharge of blood inside the human heart (Kim *et al.* 1995). Starting jets have therefore attracted a lot of attention owing to the fact that a clear understanding could result in better mechanical systems that aim to mimic their biological counterparts. Associated with starting jets from axisymmetric geometries are vortex rings, and they have been studied in great detail in the past few decades. For example, Maxworthy (1972, 1974, 1977) and Glezer (1988) have studied experimentally the properties of vortex rings. Vortex rings have been studied in the laboratory by pushing a plug of fluid out of a nozzle or orifice into quiescent fluid, also known as the 'piston–cylinder mechanism' in the literature. The outgoing flow separates at the edge of the exit, with the boundary layer on the inner walls of the cylinder rolling up to form a vortex ring. The essential features studied include the evolution of vortex rings in terms of their size, position and their circulation. Shariff & Leonard (1992) and Lim & Nickels (1995) give a comprehensive review of the earlier work done on vortex rings.

In more recent years, vortex rings have been studied with the main focus being on their association with pulsed jet propulsion in the ocean, and the unsteady blood flow in the heart. In line with this direction, the study carried out by Gharib, Rambod & Shariff (1998) asked whether there can be a limit to the maximum circulation attained by a forming vortex. In their experiments, which were done for large strokes of the piston, they showed that after the non-dimensional piston displacement ($L/d$, where $L =$ piston stroke length and $d =$ inner diameter of the cylinder) has exceeded a certain value, no additional energy or circulation entered the forming vortex ring and the remaining fluid was simply ejected as a 'trailing jet' behind the ring. The transition between these two distinct states was reported to occur at a piston stroke ratio ($L/d$) of approximately 4, which they refer to as the 'formation number'. The universality of a formation number, however, is questioned in some more recent studies. For example, Rosenfeld, Rambod & Gharib (1998) show through numerical simulations that the vortex formation number can be reduced by as much as 75 % or increased by 35 % by manipulating the temporal and spatial profiles of the cylinder exit velocity. One method to achieve this, as proposed in the numerical study of Mohseni, Ran & Colonius (2001), was to accelerate/decelerate the trailing shear layer relative to the forming vortex ring. Shusser *et al.* (2006) extended a previous analytical model on the formation of vortex rings using a piston–cylinder mechanism (Shusser & Gharib 2000) to include the effect of the piston velocity program. In the experiments carried out by Arakeri *et al.* (2004), this effect on formation number was seen for compressible vortex rings generated at the open end of a shock tube. Another method, suggested by Mohseni *et al.* (2001), for delaying the pinch-off is to increase the nozzle or orifice exit diameter as the starting flow emerges from the vortex generator. However, the experiments conducted by Dabiri & Gharib (2005*b*) show that temporally increasing the nozzle exit diameter as the starting flow develops does not necessarily delay the onset of vortex ring disconnection from the trailing jet, whereas a temporal decrease in the exit diameter increases the formation number. The interest in vortex ring disconnection from the trailing jet is because it is believed

to be significantly linked to the optimization in properties such as thrust production in pulsed jet propulsion (Krueger & Gharib 2003) and health of the human heart due to blood flow in the mitral valve (Gharib *et al.* 2006). While referring to these flows as they occur in nature, one must keep in view that these biological systems are made of flexible membranes that can deform. Motivated by these systems, we study in the present work, the formation of vortices from a piston–channel arrangement with the end of the channel having flexibility in the form of hinged leaflets. In this case, one can expect the hinged leaflets to move as a result of pressure differences across the leaflets, which will in turn affect the vortex formation at the channel exit.

Leaflets at a nozzle or orifice exit are an idealization of the heart valve and there exists a large amount of literature on different aspects of this flow. Yoganathan, He & Jones (2004) present a comprehensive review of the experimental and computational work done on the fluid mechanics of native and prosthetic heart valves. The vortex formation inside the heart was for some time believed to be an important reason behind heart valve closure, but it was shown in the study by Lee & Talbot (1979) that flow deceleration is a more important reason for the closure of the heart valves. Lee & Talbot (1979) did experiments with a dynamically and geometrically similar mechanical model of the human heart. Through direct visualization of the leaflets and pressure measurements, they showed that flow deceleration is the primary reason for an adverse pressure gradient that results in valve closure. Domenichini, Pedrizzetti & Baccani (2005) numerically studied the fluid dynamics inside a model left ventricle during diastole. Dasi *et al.* (2007), via experiments and direct numerical simulations, have studied the fluid dynamics of a bileaflet mechanical heart valve. By measurements and computations, they present detailed analysis of the leaflet kinematics and the associated vorticity dynamics. In the context of native heart valves, Pedrizzetti & Domenichini (2006) have studied numerically the flow dynamics of a two-dimensional vortex pair in the presence of a leaflet blocking the flow initially. They show that the opening of the leaflet occurs in a sequence of three phases, and present the associated fluid dynamics. Pedrizzetti & Domenichini (2007) have also studied numerically the asymmetric opening of a bileaflet valve by modelling it as a pair of rigid massless leaflets closing a two-dimensional channel. Romano, Querzoli & Falchi (2009) have done experiments with vortex pairs which are generated using a piston–channel mechanism with an orifice configuration in the presence of rectangular leaflets. They start the flow with the leaflets blocking the flow, and as the flow starts, the leaflets open out, and a vortex pair is seen forming at the exit. Inspired by the asymmetries in the heart valves, they present results with asymmetric leaflets and show the differences when compared to experiments with a single leaflet. In all these studies related to heart valves, the leaflets are initially blocking the flow, and they open as the flow starts.

Apart from heart valves, the other broad area where exit flexibility is of interest in starting jets is in the propulsion of aquatic creatures such as squids, jellyfish and scallops. The fluid mechanics of such biological propulsion has also received considerable attention, and is reviewed by Dabiri (2009). Linden & Turner (2004) study and show the existence of an 'optimal' vortex ring generated by various aquatic creatures, and define it as the ring which gives maximum thrust for a given energy input. Krueger & Gharib (2003) showed by means of direct thrust measurements that optimal thrust production is linked to the vortex ring pinch-off process. Biological systems such as squids and jellyfish have flexible and moving membranes, and this was the motivation for the study by Dabiri & Gharib (2005*b*), who used an actively controlled variable exit diameter of the nozzle to see its effect on the forming vortex

ring. Cheng & Demont (1996) studied the unsteady forces on the clapping shells of scallops from a potential flow point of view, and showed that the unsteady forces acting on the shells due to fluid reaction could be significant. It was also reported in the study by Dabiri, Colin & Costello (2006) that the velar kinematics of live jellyfish influences the formation of an optimal vortex structure. This presents an interesting opportunity to look at the effect of exit flexibility introduced in the formation process of a starting jet.

In the present work, we study the effect of hinged leaflets on the formation of a counter-rotating vortex pair. This can be thought of as an idealized problem, wherein we look at the effect of passive flexibility introduced in a starting jet. Broadly, this can have implications for understanding various biological flows, but the present work is more directly linked to biological propulsion, as explained further below. A vortex pair is a two-dimensional analogue of a vortex ring. It can be understood as a pair of counter-rotating rectilinear vortices separated by a small distance, which translates due to self-induced velocity. One of the earliest experiments on vortex pairs using the piston–cylinder mechanism, by Auerbach (1987), shows some of the essential features of this flow. He discusses the effect of exit geometry, end effects, and compares the generated vortex pair with the ring in terms of position and circulation. Recently, Afanasyev (2006) has studied the evolution of a vortex pair while maintaining two-dimensionality through stable density stratification. He presents a contrast between the vortex pair and vortex ring, showing the differences in relation to pinch-off. It is mentioned that since a clear separation of the vortex pair with the trailing jet does not occur even for $L/d = 15$, pinch-off does not take place even at this large stroke ratio. This phenomenon of the vortex pair remaining attached to the trailing jet is also reported in the numerical study by Pedrizzetti (2010), who looks at the formation process of a two-dimensional vortex pair through an orifice.

Figure 1 shows the schematic of the problem studied in this work. A vortex pair is generated using a piston–channel mechanism, which means that we push a plug of fluid out of a high-aspect-ratio rectangular duct into a quiescent medium of the same fluid. The aspect ratio is such that the dimension going into the plane of the paper (figure 1) is twenty times larger than the channel width $d$. The piston velocity ($U_p$) can be controlled as a function of time, while the channel width is kept fixed at $d$. Leaflets are introduced in the problem by hinging two rigid (non-deformable) flaps of equal length ($L_f$) at the exit of the channel. The initial position of the flaps is set parallel to the channel walls, that is, we set $\theta$ to be zero. This makes the configuration more directly related to biological propulsion as opposed to heart valves, the latter requiring the leaflets to block the flow initially. The leaflets or flaps are hinged on to the channel exit in such a manner that they are free to rotate about the channel exit as shown in figure 1. The hinge, flap material and fluid medium (water) are chosen so as to closely approximate the limiting case of negligible structural stiffness, structural damping and flap inertia, with a view to maximizing the flap opening. In this paper, we will use the words ‘leaflets’ and ‘flaps’ interchangeably, and even though the word ‘leaflets’ has been used in the literature primarily for heart valve studies, in the present work it does not reflect any direct connection with heart valves.

In the present configuration, the motion of the leaflets is purely passive, with the motion taking place only due to the pressure differences generated because of the flow. In this case, the normalized flap length, $L_f/d$, is also an important parameter. Because of the motion of the flaps, we shall see that the angle ($\theta$) changes with time (initially set as $\theta = 0°$), depending on the flow, and is directly measured in our experiments. Once the flow starts after the piston has been set into motion, the flap motions and the

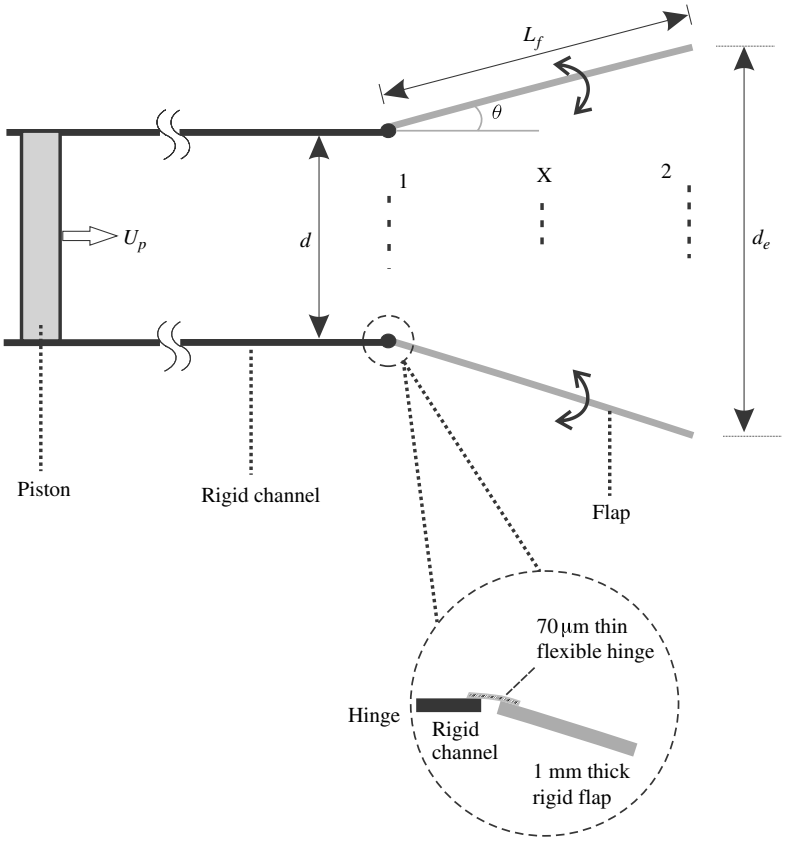


FIGURE 1. Schematic showing the arrangement used with moving leaflets at the exit and the associated nomenclature. Here, $d$ is the channel width, $d_e$ is the exit width which changes with time due to flap motion, $\theta$ is the angle subtended by the flap relative to the rigid channel wall, $U_p$ is the piston velocity, and $L_f$ is the flap length.

flow patterns hence generated were directly visualized, and flow field measurements were made using particle image velocimetry (PIV).

The layout of the paper is as follows. In § 2, we outline the experimental setup used for this study, and list the techniques used to make qualitative and quantitative measurements. In § 3, we present the results obtained using a rigid exit, that is, in the absence of any flaps. We will see that the counter-rotating vortex pair generated using a rigid exit exhibits differences when compared to the more widely studied vortex ring. In § 4, we present results from the experiments with leaflets or flaps hinged to the exit. Both measurements of the flap kinematics from direct imaging and the vorticity field from PIV measurements are presented. The former shows that the most important time scale for the flap motions is $(L/L_f)$, while the latter shows the interesting flow patterns obtained with this configuration. The effect of varying parameters such as the flap length and the piston velocity program on the flap kinematics and the flow are presented. Finally, in § 5 we shall present our conclusions from this study, providing an overview of how the presence of hinged flaps at the exit can lead to important changes in the vorticity and flow field.

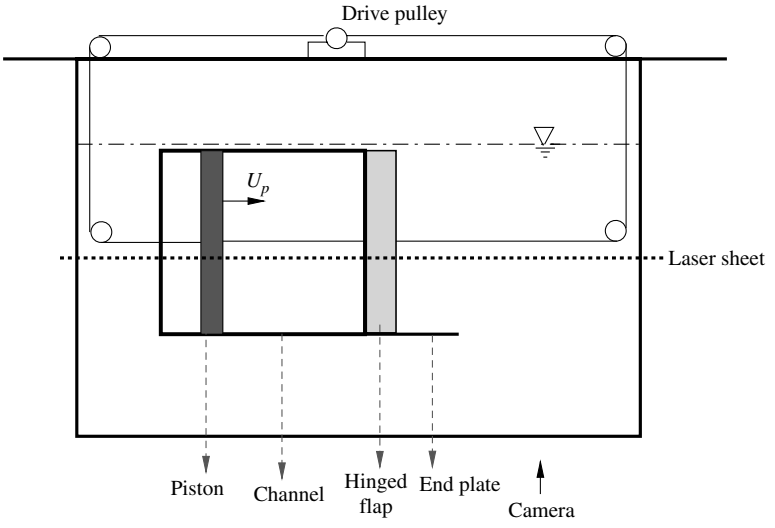


FIGURE 2. Schematic of the experimental setup used for this study.

## 2. Experimental setup

The work presented here was carried out in a free surface water tank of dimensions 120 cm (length) × 60 cm (width) × 60 cm (depth). A schematic of the experimental setup is shown in figure 2. The channel was made of 5 mm thick glass plates and was submerged in the water tank. The cross-section of the channel had the dimensions 30 cm (height) × 1.5 cm (width), which meant that the aspect ratio was 20, and it had a length of 40 cm in the direction of piston motion. The piston was made of PP polymer and was covered with a layer of sponge (1 mm thick when uncompressed) and a layer of Teflon sheet (1 mm thick) to ensure low friction and leakage-proof contact with the channel. The piston had a length of 8 cm in the direction of motion. These dimensions allowed a maximum piston stroke length of 32 cm and experiments were performed well within this limit. It was ensured that the piston was stopped at least $6d$ ($d =$ channel width) before the exit, to avoid any interaction of the flow developed on the piston face with the vortex pair forming at the exit. The piston was driven by a servomotor (Panasonic, A4 series) via a stainless steel stranded cable of 0.6 mm diameter. The cable was wound over a pulley arrangement as shown in figure 2, and was connected to the piston using small brass hooks. The servomotor connected to the pulley was controlled using a control panel which consisted of an encoder and electronics necessary to drive the servomotor. The velocity program for the servomotor was supplied to the control panel as an analogue voltage signal from a 16 bit National Instruments data acquisition card (PCI 6014) coupled to a computer. The analogue signal determined the resulting motion of the piston. To get the required velocity program for the piston, the corresponding analogue voltage signal was generated using LabVIEW software. The actual motion of the piston was checked using direct imaging of the piston motion with a high-speed camera. A sample time trace of the measured piston motion is shown in figure 3 along with the required motion (given as input to the servomotor), showing reasonably good agreement between the two.

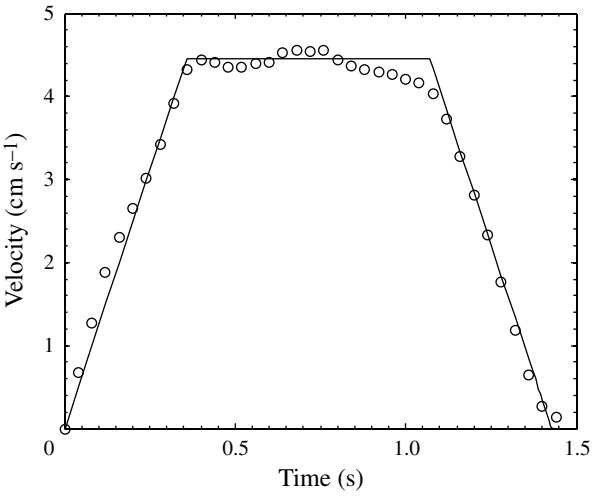


FIGURE 3. Plot showing a sample case of piston velocity as a function of time. The solid line is the expected piston motion based on the input given to the driving mechanism and the circles are the measured instantaneous piston velocity determined from imaging the piston using a high-speed camera.

An end plate of dimensions 13 cm (width) × 15 cm (length) × 1 mm (thickness) is used at the bottom of the channel exit (as shown in figure 2). This end plate along with a clean free surface at the top and a large channel aspect ratio ($AR$) of 20 helped to promote two-dimensionality. This was checked initially using dye visualizations from a side view (along the span), which showed that this configuration of an end plate at the bottom with the free surface at the top sustained a two-dimensional vortex pair for the longest time compared to other configurations tried. Such a configuration has also been used by Lisoski (1993) and Ringuette, Milano & Gharib (2007) to promote two-dimensionality of the flow, both studies being related to force measurements on accelerating normal flat plates. In particular, Lisoski (1993) studied the effect of three-dimensionality and showed that using an end plate at the bottom end and a clean free surface on the top (with $AR = 6$–$17$) generated a predominantly two-dimensional flow and suppressed the formation of tip vortices at the bottom end.

For the case with leaflets, rigid leaflets or flaps were hinged at the channel exit. The flaps were made of Perspex sheets (1 mm thick), which were cut to the required dimensions. A very thin (∼70 μm) double-sided tissue tape was used to attach the flaps at the nozzle exit. Further, the same tissue tape was made to act as a flexible hinge by leaving a small gap (∼1 mm) between the flap and the rigid exit, as shown in the inset in figure 1. It was observed that this thin hinge had low stiffness as required, with flaps displaced from their initial position, taking a large duration of time (∼30 s) to return to their initial position when compared to the maximum time scales involved in the experiments (∼3 s). The hinge stiffness was determined from the Young's modulus of the hinge material, which in turn was experimentally determined using static deflection tests of a cantilever made using the same material kept in water, with a small known point load at the edge. The Young's modulus $E$ of the hinge material determined from the experiments was close to $10^6$ N m$^{-2}$. This value was then used in the standard expression $k = EI/L_h$ to determine the order of the rotational stiffness $k$, with $I$ being the area moment of inertia of the hinge cross-section and $L_h$ the length

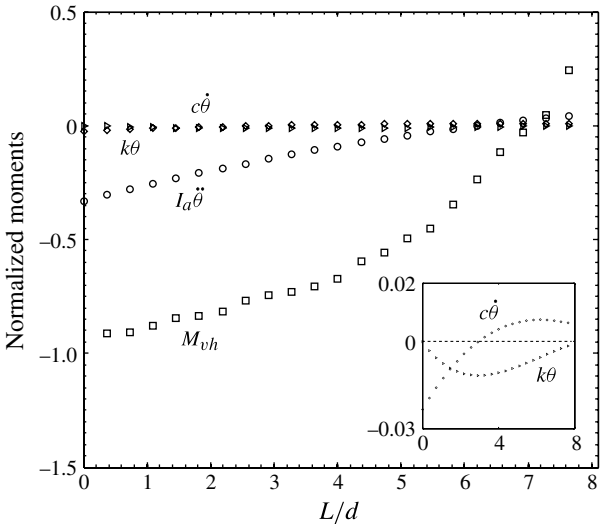


FIGURE 4. Plot comparing the moments acting on the flap due to structural stiffness ($k\theta$) and damping ($c\dot{\theta}$) with the moments caused by the fluid, for a sample case of flap motion. The moment values are normalized using the moment which arises from a fluid pressure of ($\rho {U_p}^2/2$). This case is for an impulsively started piston motion (8.19 cm s$^{-1}$) with a flap length of $L_f/d = 2$. The piston is continuously moving for the duration shown in the plot. The inset shows a close-up view of $k\theta$ and $c\dot{\theta}$, both of which are much smaller than the moments caused by the fluid ($I_a\ddot{\theta}$, $M_{vh}$).

of cantilevered hinge material. The rotational stiffness $k$ was thus found to be of the order of $7 \times 10^{-5}$ N m per metre of hinge span. The structural damping coefficient $c$ associated with the hinge material was measured by hinging a 'hollow' flap to a solid edge in air. Four 1 mm $\times$ 1 mm strips of Perspex were joined to form a 'hollow' rectangular flap with minimal fluid damping. This flap was then disturbed from its original position, and the damping coefficient was determined from the exponential decay of the resulting oscillations of the flap. The structural damping coefficient ($c$) thus determined was found to be of the order of $10^{-5}$ kg m$^2$ s$^{-1}$ per metre of the hinge span. In order to get a sense of the determined small values of structural stiffness ($k$) and damping ($c$), we compare in figure 4 the moments caused by them ($k\theta$ and $c\dot{\theta}$) against two moments caused by the fluid for a sample case of flap motion. The two moments caused by the fluid shown in the figure are due to the added moment of inertia ($I_a\ddot{\theta}$) and that due to the pressure arising from a 'velocity head' ($M_{vh}$), which develops in the channel because of the flow, both of which can be easily estimated, as discussed in more detail in § 4.1. It is clear from the plot that the fluid moments ($I_a\ddot{\theta}$ and $M_{vh}$) are substantially larger than the moments caused by structural stiffness and damping, the latter two being about two orders of magnitude smaller than the fluid moments. It should be noted that this plot does not show the moments arising due to fluid damping and vortex formation, which can in fact be quite dominant, but are harder to estimate. This plot, however, shows that the moments experienced by the flap due to the hinge's stiffness and damping are negligibly small compared to others and thus allows us to state that a 'hinged' joint of negligible stiffness and damping was achieved in the present study. Further, the ratio of the moment of inertia of the flap about the hinge ($I_f$) to its estimated added moment of inertia ($I_a$) was of the order

of 0.05, thereby suggesting that the mass of the flap (its relative density being 1.2 times the density of water) was not as crucial as the added mass associated with its geometry. In summary, the choice of the hinge, flap material and fluid medium (water) enables us to closely approximate the limiting case of a free-to-rotate rigid flap with negligible structural stiffness, structural damping and flap inertia.

The instantaneous velocity fields were measured using PIV. The flow was seeded with hollow glass spheres of 14 μm mean diameter, and the flow was illuminated by generating a laser sheet using a 15 mJ Nd:YAG pulsed laser. A Stanford Systems delay generator was used to separate in time the two laser pulses. This delay was in the range of 1–10 ms depending on the flow speed, such that it gave a maximum pixel displacement of around 5–6 pixels. The same delay generator was also used to synchronize an IDT camera (maximum resolution of $1360 \times 1036$ pixels) with the laser at desired frequencies. The acquired images were then processed using a PIV code, the details of which are given in Govardhan & Williamson (2000).

The parameters involved in this study can be noted from figure 1. The channel width ($d = 1.5$ cm) remains a constant throughout this work. The flap length ($L_f$) is non-dimensionalized with the channel exit width (to get $L_f/d$) and three different lengths, $L_f/d = 1$, 2, and 4, were used in this study. The instantaneous angle subtended by the flap with respect to the rigid channel wall is measured as $\theta$. Using this, we can also determine the instantaneous exit width $d_e$ at the flap exit. We use the widely used non-dimensional time scale $L/d$, where $L$ is the piston stroke length. In further sections, we shall refer to it as the fluid slug length as it represents the distance moved by the fluid if the fluid moved as a slug. Additional parameters are the piston velocity program (for example, impulsively started to a constant velocity or constant acceleration from rest), and the Reynolds number $Re = U_p d/\nu$, based on the magnitude of piston velocity ($U_p$) and exit width ($d$).

## 3. Rigid exit

In this section, we present results from experiments performed with a rigid exit. As an example, we start with a trapezoidal piston velocity program, where the piston is started from rest by uniformly accelerating it to some velocity followed by a constant velocity phase before the piston is brought to a halt by a uniform deceleration. In figure 5(*a*) we show vorticity contours from one such case where the maximum fluid slug length ($L/d$) reached was 5.46. The emerging flow out of the channel forms a pair of counter-rotating vortices, because of the rolling up of the separated boundary layer. A plot of the vortex centre position with time after piston stoppage is shown in figure 5(*b*). The measured translation velocity of the vortex pair ($V_o = 1.66$ cm s$^{-1}$) when compared with the velocity evaluated using the standard expression for point vortices, $V_o = \Gamma/2\pi b = 1.65$ cm s$^{-1}$ (where $\Gamma$ is the measured circulation and $b$ is the spacing between the centre of these vortices) suggests that the generated vortex pair is predominantly two-dimensional.

As the trapezoidal piston velocity program has a number of parameters, such as the duration of acceleration, deceleration and constant velocity of the piston, we conduct experiments with more basic velocity programs such as an impulsively started and an accelerating piston velocity program. In an impulsively started motion, the piston is started impulsively from rest to a particular velocity (that is, a very large acceleration) and this velocity is maintained until the piston is brought to rest impulsively. In an accelerating motion, the piston is started from rest with a constant acceleration, and this is maintained until the piston is brought to an impulsive stop. Thus, in these more basic piston velocity programs there is only one parameter, the piston velocity or the

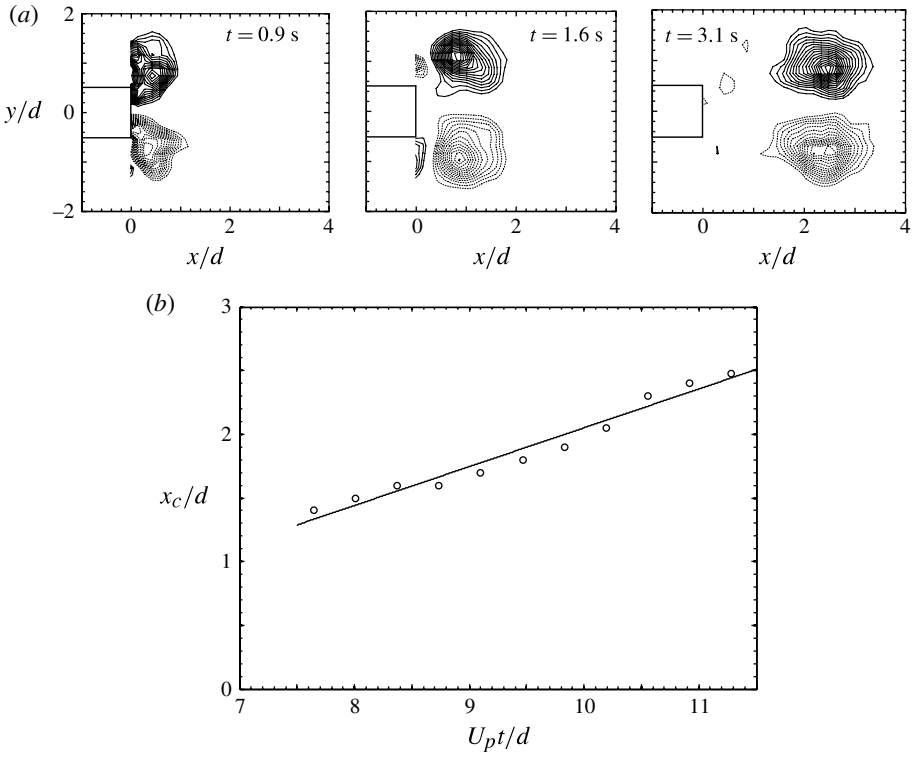


FIGURE 5. (*a*) Time sequence of vorticity contours and (*b*) a plot of vortex centre position ($x_c/d$) with time for a vortex pair generated at a rigid exit. The vorticity contours show the formation and subsequent translation of the vortex pair. The piston velocity program used is trapezoidal and the maximum $L/d$ reached is 5.46. The acceleration and deceleration durations are 0.5 s each and the constant velocity duration is 1 s. The solid and dashed lines in the contours represent opposite signs of vorticity.

piston acceleration. The work presented in the rest of this section has been carried out with large piston stroke lengths ($L/d \sim 15$). This was done to see the onset of a trailing jet and the dynamics of the flow as it develops further.

Figure 6 shows the vorticity contours for a vortex pair which was generated using an impulsively started piston velocity program. The piston is started impulsively from rest, and is kept moving until a maximum fluid slug length ($L/d$) of 15 is reached, at which it is brought to an impulsive rest. The figure shows that initially the separated boundary layer rolls up, and this process continues until $L/d$ of 8, during which there is very little motion of the vortex pair in the streamwise direction. After $L/d$ of 9, we notice that a trailing jet has begun to emerge, and the vortex pair translates forward. This is also seen in the flow visualization sequence in figure 8(*a*), where a laser sheet and fluorescein dye is used to visualize the vortex pair. This feature can also be noted by plotting the vortex position with time. As the centre of vorticity is not very clearly identifiable visually from the vorticity contours (figure 6), we use the peak in centreline $u$ velocity as an identifier of the vortex axial position. It will be shown in the next section that this method is reasonable even for more highly distributed vorticity fields. Using this method, we plot normalized vortex position ($x_c/d$) as a function of $L/d$, in figure 7(*a*). The figure shows that at around $L/d \approx 9$, the slope

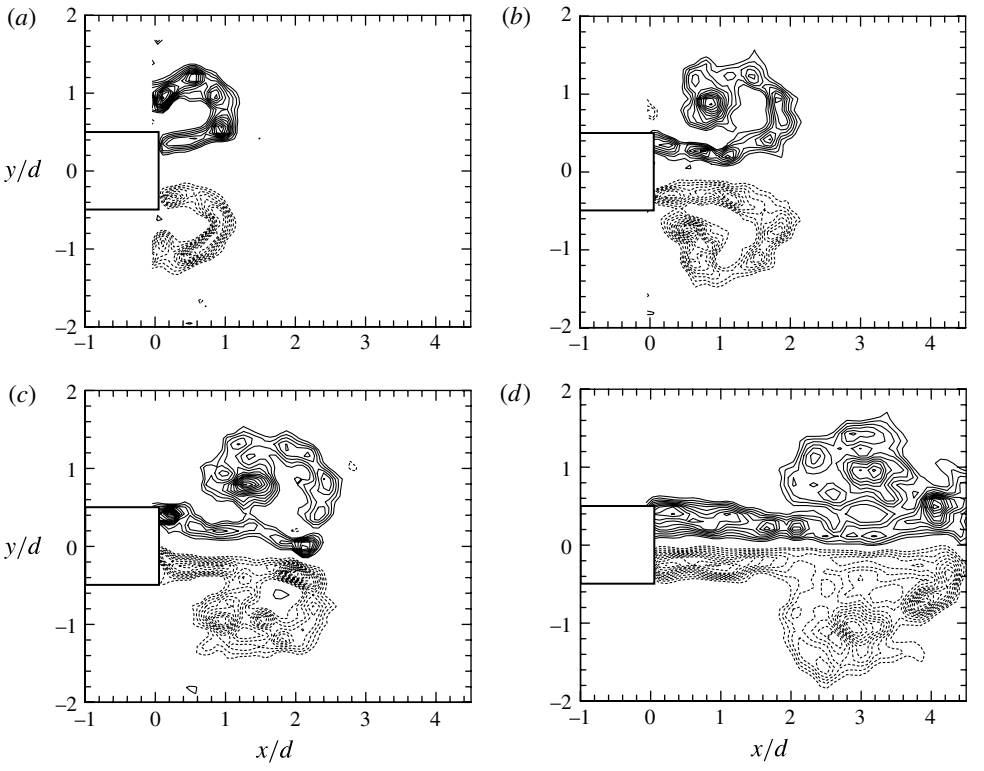


FIGURE 6. Vorticity contours for an impulsively started piston motion and a rigid exit. The piston is impulsively started and is continuously moving with a constant velocity of 5.46 cm $s^{-1}$ until a maximum $L/d$ of 15 is reached. The solid and dashed lines in the contours represent opposite signs of vorticity: (*a*) $L/d = 5.1$; (*b*) $L/d = 8$; (*c*) $L/d = 9.5$; (*d*) $L/d = 13.8$.

of the curve changes, indicating that the velocity of the vortex pair has changed from its initial value. Data from experiments at two different Reynolds number (*Re*), shown in figure 7(*a*), show no apparent effect of *Re* on this feature, at least for the range of *Re* considered. In figure 7(*b*), we plot the measured circulation as a function of time. Both the total circulation ejected and the circulation of the vortex pair are shown. Initially, the circulation of the vortex pair and the total ejected circulation are the same and both increase with time. After $L/d \approx 9$, the trailing jet is seen and the circulation of the vortex pair is smaller than the total ejected circulation. However, even after detaching from the exit, the pair is continuously fed vorticity from the trailing jet and the circulation of each vortex continues to increase with time. These results are in agreement with those of Afanasyev (2006), who also studied vortex pair generation from a rigid channel exit. He plots the position of the vortex pair front with time (figure 8 in Afanasyev 2006), and shows the existence of a 'startup time', after which the vortex pair translates forward more rapidly. These results suggest that the time scales involved in the onset of a trailing jet for a vortex pair are very different from that of an axisymmetric vortex ring, where a trailing jet is seen at $L/d \sim 4$ (Gharib *et al.* 1998). Moreover, unlike in the case of a vortex ring, the circulation of a vortex pair does not saturate, at least until $L/d \sim 15$, and it remains attached to the trailing jet as opposed to a vortex ring which detaches from the trailing jet after $L/d \sim 4$.

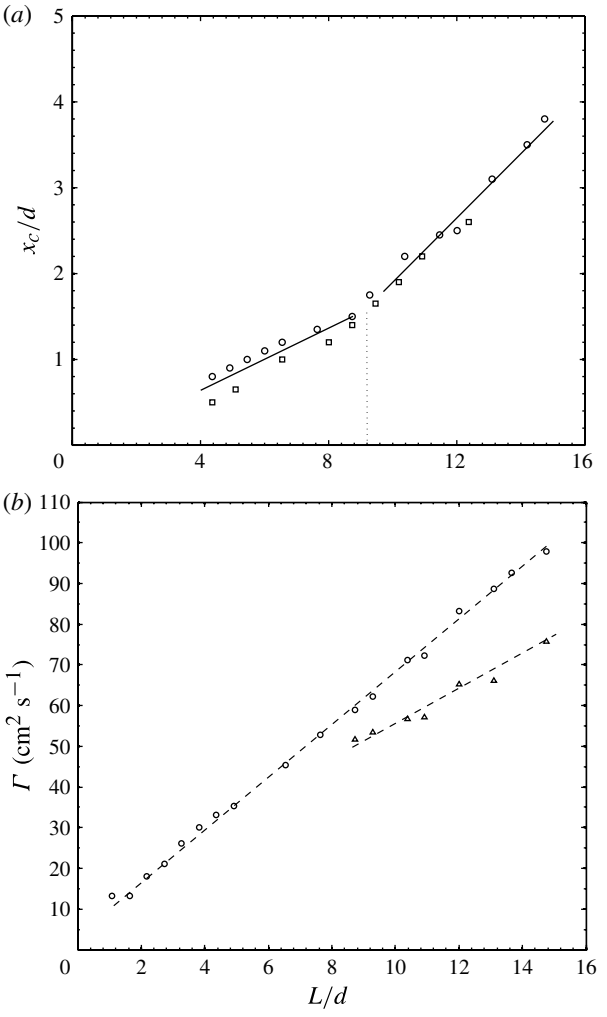


FIGURE 7. Vortex centre position ($x_c/d$ as a function of fluid slug length ($L/d$) for a rigid exit. (*a*) Vortex centre position for two different piston-velocity-based *Re*: □, $Re = 819$; ○, $Re = 1228$. (*b*) The total ejected circulation (○) and vortex pair circulation (△) are plotted for the $Re = 1228$ case. In all cases, the piston is impulsively started and is continuously moving at constant velocity.

Figure 8 shows the flow visualization sequence of a vortex pair formed using an impulsively started piston that moves with constant velocity (figure 8*a*), and an accelerating piston motion (figure 8*b*), where the piston is moving with a constant acceleration from rest. The corresponding images from (*a*) and (*b*) are both at the same fluid slug length ($L/d$). For the same fluid slug length, in the impulsively started case (*a*), the vortex pair moves farther in the downstream direction when compared to case (*b*). Also, the onset of a trailing jet is delayed in case (*b*). This dependence of onset of a trailing jet on the piston velocity program was predicted in the computational study by Mohseni *et al.* (2001) for axisymmetric vortex rings. Such behaviour was also reported in the experimental study by Arakeri *et al.* (2004) for vortex rings generated at the open end of a shock tube. However, a clear and

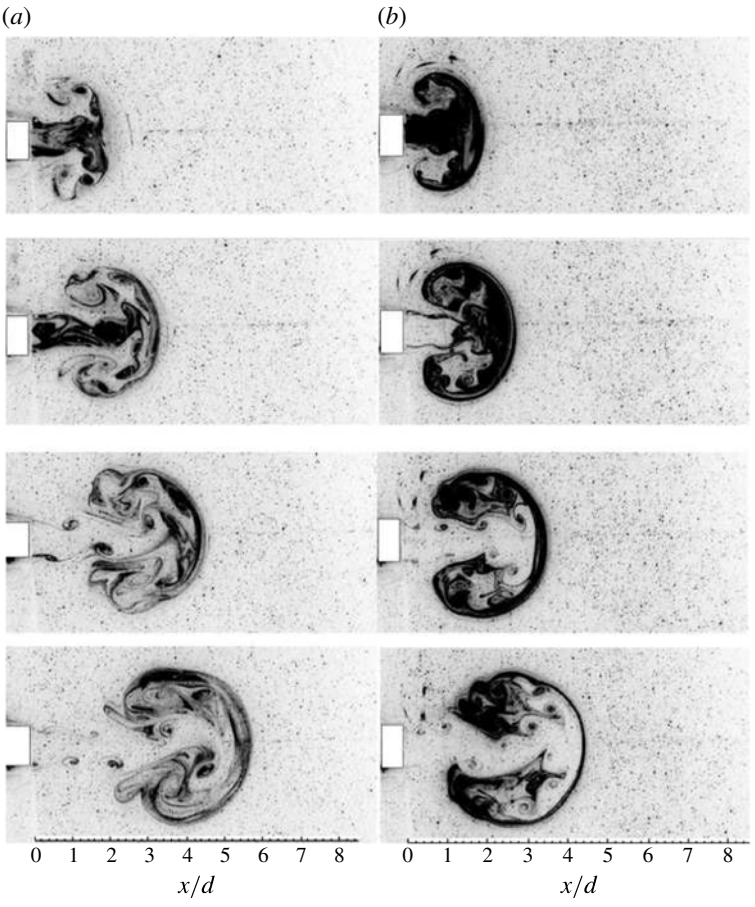


FIGURE 8. Flow visualization sequences to compare impulsive and accelerating piston motion. (*a*) The piston is impulsively started and is continuously moving with a constant velocity of 5.46 cm $s^{-1}$. (*b*) The piston is moving continuously with an acceleration of 7 cm $s^{-2}$. In both cases the images shown are at approximately $L/d = 6, 9, 12$ and 15, and hence side-by-side images are at the same fluid slug length. A maximum $L/d$ of 15 is reached before the piston is brought to rest impulsively in both cases.

quantitative dependence on the piston velocity program would need more experiments with this objective in mind. Qualitatively, it can be said that by accelerating the piston, the vortices formed tend to cover less streamwise distance compared to when the piston is moving with a constant velocity for the same ejected fluid slug length. In contrast, although not shown here, we observe that for a decelerating piston motion (i.e. the piston is started impulsively and then decelerated uniformly to rest) the effect is opposite, that is, the vortices cover more streamwise distance as compared to when the piston is moving with a constant velocity.

## 4. Exit with hinged leaflets

In this section, we present results from experiments performed with hinged leaflets at the exit. As mentioned in § 1, the configuration of the hinged system used in

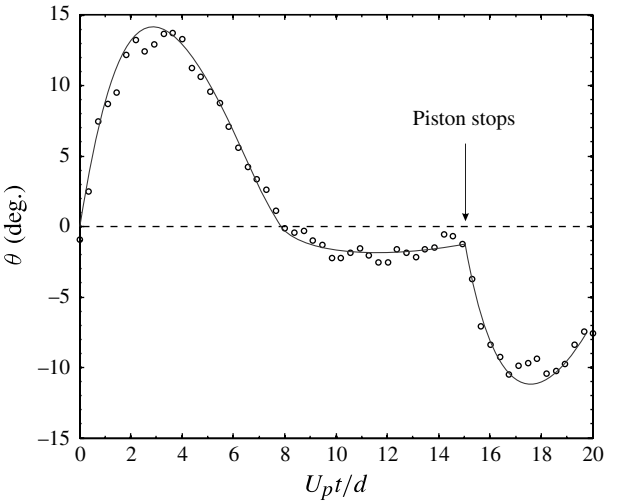


FIGURE 9. Plot of flap angle ($\theta$) with time for $L_f/d = 2$. The piston velocity program is impulsively started, with $U_p = 8.19$ cm s$^{-1}$. The maximum fluid slug length reached is 15, i.e. the piston stops impulsively at $U_p t/d = 15$.

our experiments closely approximates the case of a free-to-rotate rigid flap with negligible structural stiffness, structural damping and flap inertia. The configuration thus represents a limiting case from the structural side, with the flap kinematics being decided almost completely by the unsteady fluid moments acting on the flap. Before each experiment, the flaps are placed parallel to the channel walls, i.e we set $\theta = 0°$. With this initial condition, the piston is moved with a prescribed velocity program and the flaps move as dictated by the fluid forces acting on them. Experiments were done with different piston velocity programs and with three different flap lengths.

We begin by presenting in figure 9 a typical measured variation of the flap angle ($\theta$) with time corresponding to an impulsive piston velocity program. The typical motion of the flaps involves a rapid opening as the flow starts, a gradual slowdown to a maximum opening angle ($\theta_{max}$), followed by a more gradual return of the flap towards its initial position. The measurements show that at larger times, the flaps asymptote towards a small negative angle with the flaps staying in this position as long as the piston is in motion. This is followed by a rapid closure of the flaps when the piston stops.

Having seen the typical flap motions, we present in figure 10 sample flow visualization sequences to illustrate the additional flow features observed in the hinged leaflet cases. The sample cases shown correspond to two different flap lengths, (*a*) $L_f/d = 2$ and (*b*) $L_f/d = 4$, both done with trapezoidal velocity programs. The sequences show the possibility of formation of three different pairs of vortices, which we refer to as A, B and C. These are shown schematically in figure 11 for clarity, and are discussed below.

The vortex pair A would be the only vortices formed if the flaps did not move. These are formed because the boundary layer formed on the inner surfaces of the flaps separates at the tip, and is thus analogous to the vortex pair formed in the rigid exit case. The additional pairs B and C are the ones caused by the motion of the flaps. The vortex pair B forms due to flow separation at the hinge when the flap has opened. The

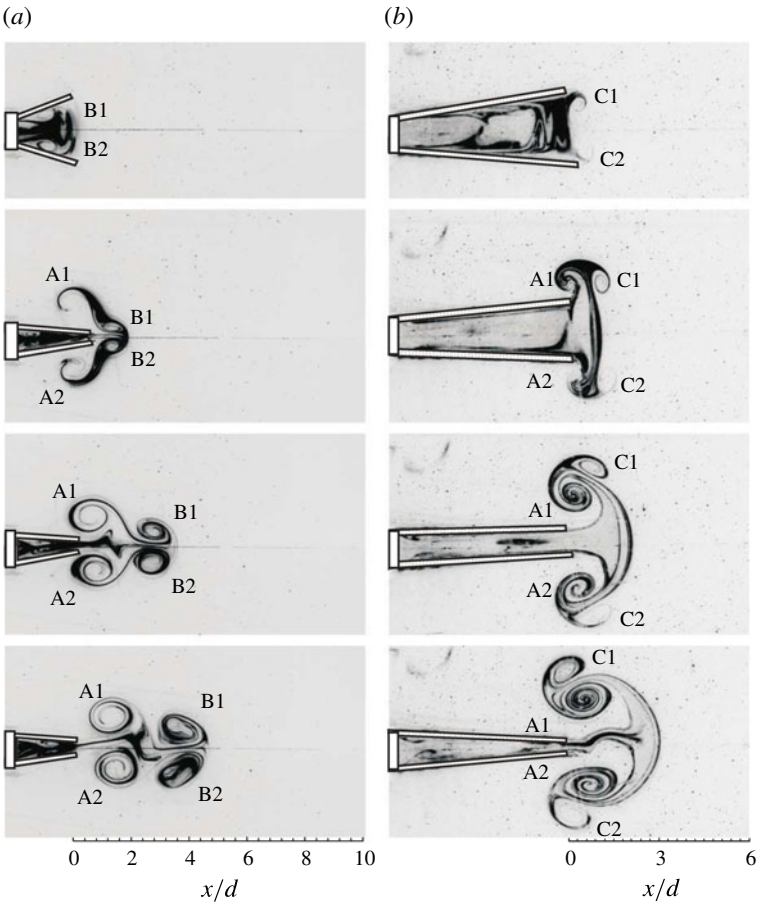


FIGURE 10. Flow visualization sequences for (*a*) $L_f/d = 2$ and (*b*) $L_f/d = 4$. For both the cases, the piston velocity program is trapezoid with an initial acceleration time of 0.5 s, and then a phase of constant velocity for 1 s and eventually deceleration to stop in 0.5 s. The maximum piston velocity reached is approximately 5.46 cm $s^{-1}$ and the final fluid slug length ($L/d$) is 5.4.

separated flow at the hinge point (figures 11*b* and 10*a*) because of an adverse pressure gradient (similar to that in a diffuser) forms a pair of vortices (B1 and B2) with the same sign as that of A1 and A2 respectively, and these translate forward. Another pair of vortices (C1 and C2) also form during flap opening, but are formed due to separation of the boundary layer vorticity on the outer surface of the flap (figures 11*a* and 10*b*). Vortices C are similar to those which would be produced if the flaps were moved outwards in a quiescent fluid. Since the boundary layer on the outer surface of the flap would have vorticity with the opposite sign to that on the inner surface, the resulting vortices (C) also have the opposite sense compared to the vortex pairs A and B. The relative strength of vortex pair C was found to be dependent on the flap length, with the shorter flaps producing stronger C vortices because of their rapid opening. These vortices are not seen in figure 10(*a*) because of the absence of dye in the flap region. In general, all three vortex pairs (A, B and C) will be generated in each leaflet case, although their individual strengths may vary.

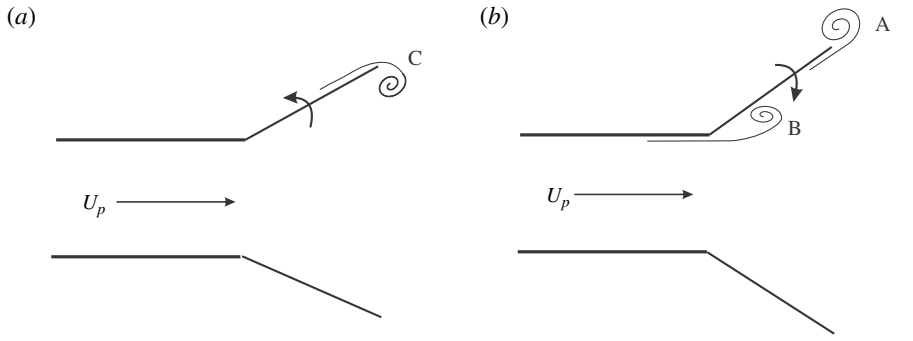


FIGURE 11. Schematic showing the different kinds of vortices formed with hinged leaflets. Vortices on only one side of the channel are sketched for clarity. Also, all three pairs of vortices A, B and C can form simultaneously during leaflet opening, but these have been sketched separately in (*a*) and (*b*) for clarity.

As in § 3, we note that a trapezoidal piston velocity program has many parameters, such as the durations of acceleration, deceleration and constant velocity of the piston. Thus, henceforth we will present results from experiments done using more basic piston velocity programs. We shall in particular focus our attention on the simple impulsively started program with constant velocity for most of this section, with some results also presented from the constant acceleration program. In the present configuration, the flaps introduce only one parameter, which is the flap length ($L_f$), since the flap inertia ($I_f$), structural stiffness ($k$), and structural damping ($c$) are negligible. The only other relevant parameters are the piston velocity ($U_p$) or acceleration ($a$), the channel width ($d$) and viscosity ($\nu$).

We shall first present in § 4.1 the measured flap kinematics for different flap lengths and piston velocities. In § 4.2, we define a new time scale based on the flap length ($L_f$) and show that it is useful in collapsing the observed flap motion data for different flap lengths. We shall subsequently present in § 4.3 the vorticity dynamics associated with the flap kinematics, and will give an overview of how the two are coupled.

### 4.1. *Leaflet kinematics*

We will now look systematically at the kinematics of the flaps. We shall focus here on the impulsively started piston velocity program with constant velocity, and present data for varying piston velocity ($U_p$) and flap length ($L_f$).

In figure 12 we present a plot of flap angle as a function of time for an impulsively started piston velocity program with $L_f/d = 2$. The plot contains data from a range of piston velocities (8.2–16.3 cm s$^{-1}$). In each case, data is shown only when the piston is in motion, and hence the closing of the flaps related to piston stopping seen earlier in figure 9 is not seen. In all cases shown, the nature of the flap angle variation with time is very similar, and, as discussed earlier, involves a rapid opening of the flap, a gradual approach to a maximum angle ($\theta_{max}$) and then a slow inward movement of the flaps. It is also clear from the figure that the kinematics of the flaps does not appear to be significantly affected by the piston velocity over the range of velocities considered in the present experiments (*Re* based on $U_p$ from 819 to 2457). In all cases, the flaps are found to reach the same maximum opening, $\theta_{max} \approx 15°$, at $L/d \approx 3$.

The effect of varying flap length ($L_f/d$) on the flap kinematics is shown in figure 13. All three sets of data correspond to the same impulsive piston velocity

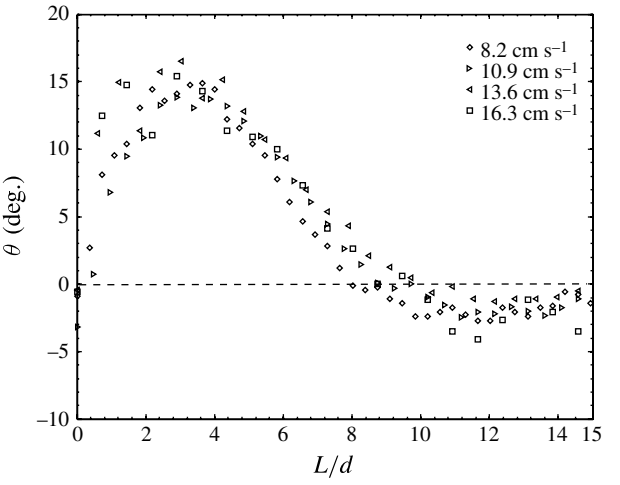


FIGURE 12. Plot of flap angle with fluid slug length for $L_f/d = 2$. The piston velocity program is impulsively started and the maximum fluid slug length ($L/d$) is 15. The plot contains data from different magnitudes of piston velocity.

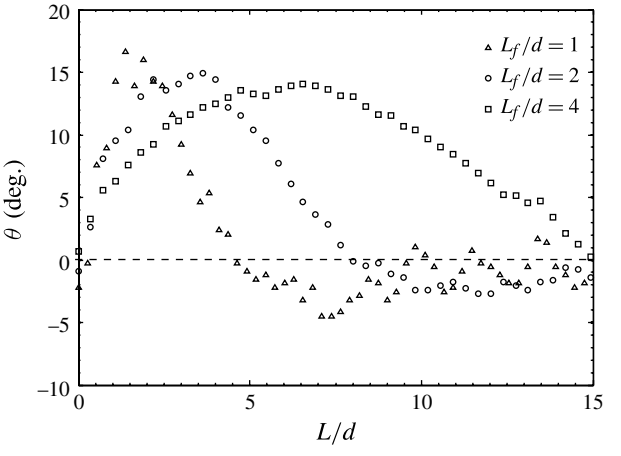


FIGURE 13. Plot of flap angle with fluid slug length ($L/d$) for different flap lengths. The maximum fluid slug length ($L/d$) is 15 and the piston velocity program used is impulsively started, with the magnitude of piston velocity being 8.19 cm s$^{-1}$ for all cases.

program ($U_p = 8.19$ cm s$^{-1}$). The maximum opening angle ($\theta_{max}$) and the trends in the three cases shown are found to be similar. However, there are large changes in the time at which the flaps reach maximum opening and the time when they return to their initial position. For example, the maximum opening occurs at $L/d \approx 2$ for $L_f/d = 1$, at $L/d \approx 4$ for $L_f/d = 2$, and at $L/d \approx 7$ for $L_f/d = 4$. Clearly the time for flap opening and closing vary widely when the conventionally used non-dimensional time scale ($L/d$) is used. Table 1 lists the essential data obtained from experiments done for different flap lengths with an impulsively started piston motion.

| Impulsively started | $L_f/d = 1$ | $L_f/d = 2$ | $L_f/d = 4$ |
|---|---|---|---|
| $\theta_{max}$ | 15.5° | 14.5° | 13.5° |
| $(d_e/d)_{max}$ | 1.7 | 2.1 | 2.54 |
| $L/d$ for $\theta_{max}$ | 1.4 | 2.5 | 7 |
| $L/d$ for $\theta = 0°$ | 4.7 | 9 | >15 |

TABLE 1. Important flap kinematics data for different flap lengths with an impulsively started piston motion. The values listed are averaged for Reynolds number ranging from 819 to 2457.

With a view to understanding the observed flap kinematics, we shall now look at the governing equation for the flap motions. The flap motion is determined by the flap angle ($\theta$), which in general is governed by the equation

$$(I_f + I_a)\ddot{\theta} + c\dot{\theta} + k\theta = M, \tag{4.1}$$

where $I_f$ is the moment of inertia of the leaflet, $I_a$ is the added moment of inertia for the leaflet geometry, $c$ is the structural damping coefficient and $k$ is the structural stiffness associated with the hinge. The moment $M$ on the right-hand side here is the summation of all the moments arising due to fluid forces, except that due to the added moment of inertia ($I_a\ddot{\theta}$), which is written separately on the left-hand side of the equation. As already discussed in § 2, in all our cases $I_f \ll I_a$, and the moments caused by $c\dot{\theta}$ and $k\theta$ are very small compared to the moments caused by $M$, and hence the governing equation for the motion becomes

$$I_a\ddot{\theta} = M. \tag{4.2}$$

It should be noted that $I_a$ would in general be a function of time, as is the case with many unsteady flows. Further, one would expect the flow immediately after flow initiation to be like potential flow, and the value of $I_a$ at very small times would be the same as the potential flow value.

We now present a simplified one-dimensional unsteady inviscid flow analysis to get a sense of the moments acting on the flaps. The one-dimensional flow analysis presented below has similarities to the potential flow model developed by Cheng & Demont (1996) for studying the unsteady moments on the clapping shells of scallops. However, it should be noted that the present analysis does not take into account flow separation and vortex formation, which will certainly alter the flow and the associated flap kinematics.

We apply continuity and Bernoulli's equations between stations 1 and 2 (see figure 1). Applying continuity, we get

$$U_e d_e = U_p d - U_{tip} L_f, \tag{4.3}$$

where $U_{tip}$ is the instantaneous flap tip velocity ($=L_f\dot{\theta}$) and $U_e$ is the (average) exit velocity. The above equation shows that the exit velocity ($U_e$) is reduced, as some part of the flow from the channel goes to fill the space opened up by the outward flap motion on both sides. It is thus possible even to get a negative value of $U_e$ if the flaps open rapidly enough. This would mean that there can be conditions when the ambient fluid might be drawn into the flap region, and this is discussed more later.

Further, applying Bernoulli's equation between the intermediate station X and station 2 with respect to figure 1 gives us

$$\left(\frac{p_x - p_2}{\rho}\right) = \int_x^{L_f} \frac{\partial u_x}{\partial t}\,\mathrm{d}x + \left(\frac{{u_2}^2 - {u_x}^2}{2}\right). \tag{4.4}$$

This equation would determine the pressure acting on the inside surface of the flaps, for this ideal situation of a one-dimensional inviscid flow. This pressure consists of two terms, the first term on the right-hand side is the unsteady term that would contribute towards creating a positive pressure gradient as the flow starts from rest, resulting in an outward moment on the flaps about the hinge. This may also be thought of as the pressure gradient developed to accelerate the fluid slug contained between the flaps. At small times, the moment due to this high pressure between the flaps (similar to over-pressure observed during formation of vortex rings by Krueger 2005) is balanced by the moment due to the added moment of inertia term ($I_a\ddot{\theta}$). The rapid closing of the flaps when the piston stops is caused by the same phenomenon as flap opening, which in this case leads to an under-pressure within the channel. This is similar to the observations made by Lee & Talbot (1979), who note that the closure of the valves in a dynamically similar model of the heart is due to flow deceleration. To understand why the flaps tend to move back to their initial position, we need to consider the second term on the right-hand side which is the 'velocity head' term. Here, $u_x$ at any location can be evaluated from the continuity equation (4.3). As the flaps open, from continuity we know that the velocity at the hinge point would be larger than at the exit. This would result in lower pressure at the hinge point compared to that at the exit. This would in turn result in an inward moment on the flaps about the hinge (referred to as $M_{vh}$ in figure 4). The return of the flaps after reaching $\theta_{max}$ is also consistent with the case of a steady jet issuing out through the flaps, where one would expect the flaps to be nearly parallel to the rigid walls ($\theta \approx 0$). In reality, however, as shown earlier in figure 10, the flow is more complex with separation and formation of various types of vortices that would definitely affect the forces on the flaps and hence the motion of the flaps.

For small times, $t = 0^+$, the flow is expected to be like potential flow, as flow separation and vortex formation would take finite time. Hence, estimates from potential flow at small times should compare well with measurements. At small times, the moment on the flaps due to the unsteady pressure term in (4.4) would be balanced by the added moment ($I_a\ddot{\theta}$) as shown by

$$I_a\ddot{\theta} = \rho \int_0^{L_f} \left\{ \int_x^{L_f} \frac{\partial u_x}{\partial t}\,\mathrm{d}x \right\} x\,\mathrm{d}x. \tag{4.5}$$

The flap tip velocity at initial time ($U_{tip}|_{t=0^+}$) can be obtained by integrating the above equation from $t = 0$ to $t = 0^+$, during which the piston velocity changes from zero to $U_p$ for the impulsively started case. The value of $u_x$ can be determined from continuity, and we assume a standard form for the added moment of inertia, $I_a = k_a\rho L_f^4$, where $k_a$ is a constant corresponding to our flow geometry. Using these, we can obtain an expression for the velocity of the flap tip at flow initiation as

$$U_{tip}|_{t=0^+} = L_f\dot{\theta}|_{t=0^+} = \frac{U_p/6}{(k_a + L_f/10d)}. \tag{4.6}$$

It should be mentioned here that at these small times the above estimate should be close to the real experimental case, as the flow is very close to potential at these

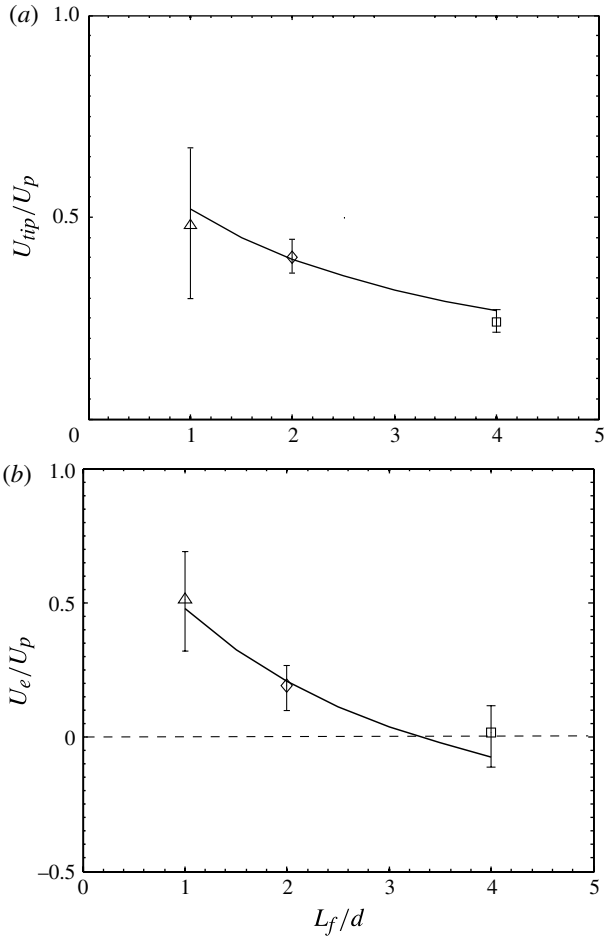


FIGURE 14. (*a*) Plot showing the flap tip velocity ($U_{tip}/U_p$) for different flap lengths at small times after flow initiation. $U_{tip}$ is evaluated by using the measured flap angle ($\theta$) with time. The solid line represents the evaluated $U_{tip}$ using (4.6). (*b*) Plot showing the exit velocity ($U_e/U_p$) for different flap lengths at small times after flow initiation. $U_e$ is evaluated by using the measured flap angle ($\theta$) with time. The solid line represents the evaluated $U_e$ using (4.3) and (4.6). In both (*a*) and (*b*), data from different piston velocities is averaged for each flap length, and the bar shows the spread of data. The velocity program is impulsively started in both the plots.

small times, as already discussed. Figure 14(*a*) shows the plot of $U_{tip}|_{t=0^+}$ determined from the experimental measurements of the flap motion, normalized in each case by the piston velocity $U_p$. The plotted symbol is a mean for different piston velocity cases and the length of the bar shows the spread of the measured data for different piston velocities. The estimate for $U_{tip}|_{t=0^+}$ can be obtained from (4.6) if the added moment coefficient $k_a$ is known for our geometry. We find that using $k_a = (9\pi/128)$, which corresponds to that for a plane lamina rotating about one edge (Brennen 1982), gives a reasonable match with the measurements. This is shown by the solid line in figure 14(*a*) which is evaluated using (4.6) for different flap lengths. Figure 14(*b*) shows the plot of exit velocity at $t = 0^+ (U_e|_{t=0^+})$ as a function of flap length. The

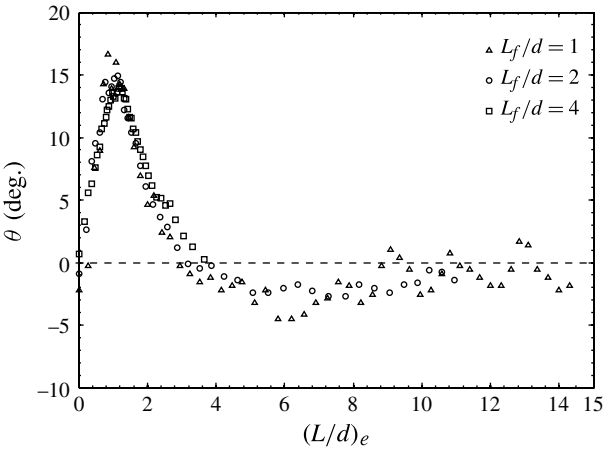


FIGURE 15. Plot of flap angle with effective fluid slug length $(L/d)_e$ for different flap lengths. The maximum fluid slug length $(L/d)$ is 15 for both cases, and the piston velocity program used is impulsively started, with the magnitude of piston velocity being 8.19 cm s$^{-1}$ for all cases.

symbols represent $U_e|_{t=0^+}$ obtained from the measured flap tip velocity ($U_{tip}|_{t=0^+}$) and continuity equation (4.3), and the bar indicates the spread of data for different piston velocities. The solid line is the exit velocity determined using (4.3) and (4.6). As stated earlier, we note from continuity equation (4.3) that for sufficiently fast opening of the flaps there can even be a reverse flow at the exit point ($U_e < 0$). This is in fact seen in figure 14(*b*) for $L_f/d = 4$, where for certain piston velocities a reverse flow is indeed seen at the flap exit. The measured velocity field for such a case is also shown later in § 4.3.

### 4.2. *Time scale for leaflet kinematics*

We next look at what would be an appropriate time scale for the flap kinematics. Dabiri & Gharib (2005*a*) have defined a time scale for flows with time-dependent width of the exit. Such a time scale is formulated by integrating the incremental fluid slug length over a period of piston motion. This would result in an effective fluid slug length $(L/d)_e$, which can be written as $\int_0^t u_e \, \mathrm{d}t/d_e$, where $u_e$ and $d_e$ are the instantaneous velocity at the flap exit and the exit width respectively, and $t$ is the time from the start of piston motion. For rigid exits, where $d_e(=d)$ is fixed, this would reduce to the conventional slug length $(L/d)$. In our experiments with hinged flaps, $u_e$ is estimated from mass conservation using the exit width $(d_e)$ obtained from flap visualizations. The effective fluid slug length $(L/d)_e$ can thus be calculated only after the experiments and is not known *a priori*. Figure 15 is the plot of flap motion for three different flap lengths, all with the same impulsively started piston velocity program ($U_p = 8.19$ cm s$^{-1}$) using the effective fluid slug length $(L/d)_e$ as a time scale. Figure 15 shows that the instant of maximum opening ($(L/d)_e \approx 1$) and the instant at which the flaps return to their initial position ($(L/d)_e \approx 3.5$) seem more or less independent of the flap length. Further, although only one piston velocity case ($U_p = 8.19$ cm s$^{-1}$) is shown in figure 15, there is little variation with the magnitude of piston velocity as was shown in figure 12 for the range of $Re$ considered. This indicates that the nature of figure 15 is reasonably representative of all the piston velocity cases studied. It should be noted again that $(L/d)_e$ is not an independent

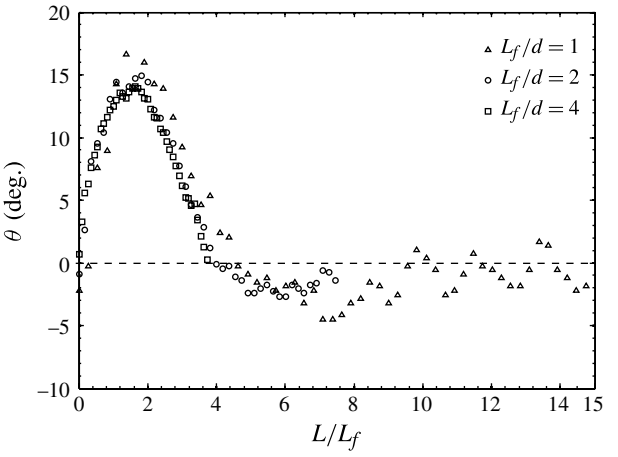


FIGURE 16. Plot of flap angle with $L/L_f$ for different flap lengths. The maximum fluid slug length ($L/d$) is 15 and the piston velocity program used is impulsively started, with the magnitude of piston velocity being 8.19 cm s$^{-1}$ for all cases.

parameter in our experiments, as an *a priori* knowledge of this is unavailable, and it can only be determined from measurements of $\theta$ with time. Thus, it would be interesting if we can introduce a length scale and time scale that would not only collapse the data but also make physical sense and be known *a priori*. Keeping this in view, we now look at the dimensional analysis of the unsteady Bernoulli equation (4.4). We can take the piston velocity $U_p$ as a velocity scale for an impulsively started program (such that $u_x^* = u_x/U_p$), $L_f$ as a length scale (such that $x^* = x/L_f$), and normalize time as $t^* = t/\tau$ for impulsively started motion. Now, if we seek to normalize (4.4) we get

$$(p_x - p_2)^* = \left(\frac{L_f}{\tau U_p}\right) \int_0^1 \frac{\partial u_x^*}{\partial t^*}\, \mathrm{d}x^* + \left(\frac{u_2^{*2} - u_x^{*2}}{2}\right), \tag{4.7}$$

thereby suggesting that a non-dimensional time scale $t^* = t/\tau$ can be defined by taking $\tau = L_f/U_p$. This implies that $t^* = L/L_f$. We present in figure 16 the flap kinematics plotted versus this new time scale ($L/L_f$). The plot shows a reasonably good collapse of the data for all three flap length cases studied. In all cases, the time at which the flaps reach maximum opening is $L/L_f \sim 1.75$, while the time at which they return to their initial position is $L/L_f \sim 3.75$. This suggests that as long as the flaps are moving, the length of the flaps becomes an important length scale in the impulsively started piston motion cases, and the kinematics across all flap lengths and all the piston velocities studied here collapses into a single motion when $L/L_f$ is used as the time scale.

Although $L/L_f$ as a time scale collapses the flap kinematics well for impulsively started piston motion, this is not always the case. When we use an accelerating piston motion the kinematics of the flap does not collapse as well. In figure 17 we use the time scale $L/L_f$ for plotting the flap kinematics across different flap lengths in an accelerating piston motion case. Also drawn for comparison is a trend line for an impulsively started piston motion representative of all flap lengths. Even though $L/L_f$ brings the data closer as compared to when we use $L/d$ as the time scale (not shown here), a collapse like that in figure 16 is not observed. It is also observed that the

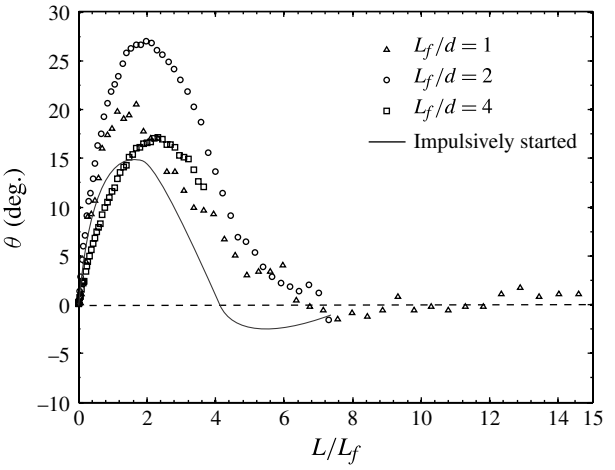


FIGURE 17. Plot of flap angle with $L/L_f$ for accelerating piston velocity program (with an acceleration of 7 cm s$^{-2}$) for different flap lengths. A typical flap motion for impulsively started velocity program is sketched for comparison.

| Accelerating | $L_f/d = 1$ | $L_f/d = 2$ | $L_f/d = 4$ |
|---|---|---|---|
| $\theta_{max}$ | 20.5° | 27° | 16.5° |
| $(d_e/d)_{max}$ | 1.7 | 2.8 | 3.2 |
| $L/d$ for $\theta_{max}$ | 1.5 | 4 | 9.3 |
| $L/d$ for $\theta = 0°$ | 7.9 | 12.7 | >15 |
| $L/L_f$ for $\theta_{max}$ | 1.7 | 2 | 2.2 |
| $L/L_f$ for $\theta = 0°$ | 6.5 | 7 | >4 |
| $(L/d)_e$ for $\theta_{max}$ | 0.85 | 1 | 2 |
| $(L/d)_e$ for $\theta = 0°$ | 4 | 4 | >2.5 |

TABLE 2. Important flap kinematics data for different flap lengths with an accelerating piston motion. The values listed are averaged and for values of acceleration ranging from 7–15 cm s$^{-2}$.

maximum opening angle changes significantly with flap length. Although not shown here, it may be noted that there is no significant change in the flap kinematics with varying values of acceleration for the range studied (7–15 cm s$^{-2}$). The values of $\theta_{max}$, the time taken to reach $\theta_{max}$ and the time taken to return to initial position with various time scales for the accelerating piston cases are tabulated in table 2.

### 4.3. *Vorticity dynamics*

As seen earlier in figure 10, the vorticity dynamics of the fluid issuing out of a channel is significantly altered by the introduction of hinged leaflets.

We now look systematically at the vorticity dynamics associated with the leaflet motions. First, we look at the nature of the flow at small times. Figure 18 shows the instantaneous velocity field at flow initiation for a sample case where the piston is impulsively started from rest. As discussed earlier, at very small times we would expect the flow to be potential with the absence of any vortices. Also, as noted before, using continuity equation (4.3) we find that at flow initiation there can be a reverse

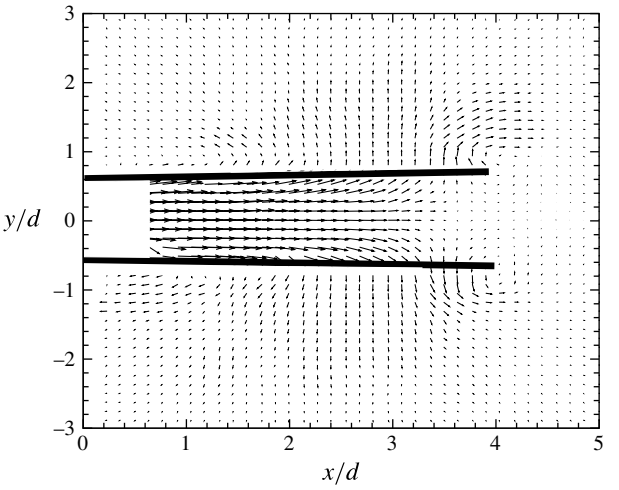


FIGURE 18. Velocity vectors for hinged leaflets ($L_f/d = 4$) with impulsively started piston motion ($U_p = 5.46$ cm s$^{-1}$). This velocity field is at a fluid slug length ($L/d$) of approximately 0.4. The flaps are moving out, causing a reduction in the velocity along the streamwise direction in the region between the flaps.

flow at the flap exit due to rapid opening of the flaps. This is seen to some extent in figure 18, where the flow coming out of the channel bends to fill in the space created by the outward motion of the flaps, with an indication of a small reverse flow at the flap exit. The flow outside the flaps at these early times also seems potential-like, with the gradual formation of vortices a little later. It can thus be said that the forces on the leaflet at initial times would be dominated by the unsteady pressure from (4.4).

We next look at how the flow develops at later times. In figure 19 the vorticity contours are shown at a time when the leaflets have reached their maximum opening angle ($L/L_f \approx 2$), for all three flap lengths. The flow looks qualitatively similar across the three flap lengths, with the exception of stronger C vortices (with reference to figure 11) in the $L_f/d = 2$ case. The formation of vortices A at the flap tip is in its preliminary stage in all three cases. However, the separation at the hinge point and the formation of B vortices can be seen more clearly in the longer leaflet cases. Having looked at the effect of flap length, we present in figure 20 a time sequence of vorticity plots for the $L_f/d = 4$ case, with an impulsively started piston velocity program ($U_p = 5.46$ cm s$^{-1}$). The sequence shows the development of vorticity while the piston is in motion. The initial opening of the flaps results in flow separation at the hinge end and the formation of a pair of counter-rotating vortices (referred to as B in figure 11). Another point of flow separation is at the tip of the flaps, which also results in the formation of a vortex pair (referred to as A). This pair is similar to that formed with a rigid exit. The vortices referred to as C are weak in this case and are not seen clearly in the vorticity plot. Figure 20 shows that even at later times these vortices (A and B) remain distinct.

Although the time scale ($L/L_f$) collapses the data for the different flap lengths ($L_f/d$) in figure 16, there are significant differences in the vorticity distribution outside the flaps with flap length, as shown by the vorticity plots in figure 21. All the vorticity plots shown in the figure are taken at $L/L_f \approx 3.75$, which corresponds to the instant when the flaps return to their initial position in each case. The figure shows that as the

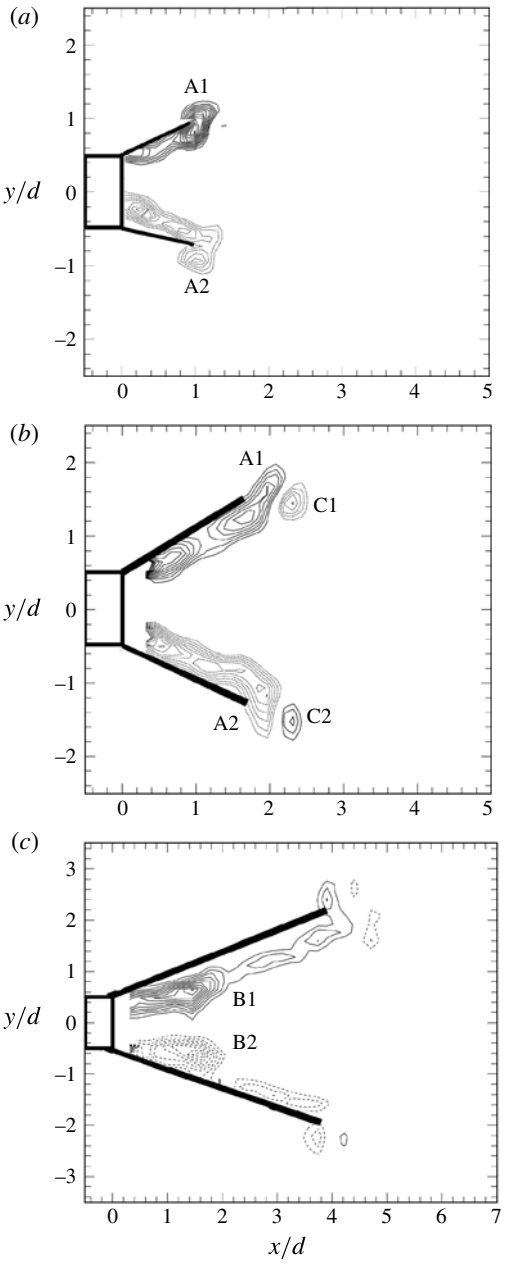


FIGURE 19. Vorticity field for hinged leaflets with an impulsively started piston motion: (*a*) $L_f/d = 1$; (*b*) $L_f/d = 2$; (*c*) $L_f/d = 4$. In all three cases, $L/L_f$ is approximately 1.75, i.e. the leaflets have reached their maximum opening angle.

flap length increases, the vorticity is distributed over a larger physical region, resulting in more clear separation of vortices A and B. Although the reasons for the differences are not completely clear, it may be related to the longer physical time associated with the motions of the larger flaps, which could provide additional time for flow separation

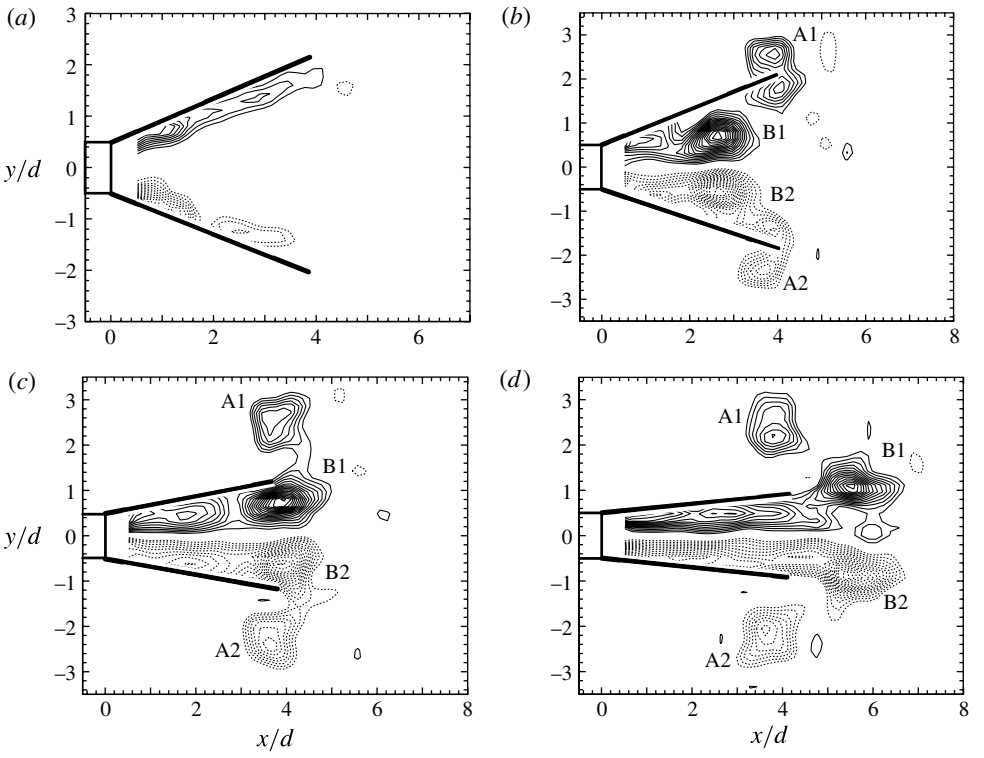


FIGURE 20. Vorticity contours for hinged leaflets ($L_f/d = 4$) with impulsively started piston motion. The piston is impulsively started and is continuously moving with a constant velocity of 5.46 cm s$^{-1}$. The solid and dashed lines in the contours represent opposite signs of vorticity: (*a*) $L/d = 5.1$; (*b*) $L/d = 9.8$; (*c*) $L/d = 11.6$; (*d*) $L/d = 14.2$.

at the hinge. Also shown on the top side of each vorticity plot in figure 21 is the streamwise length ($x$) normalized by the flap length ($L_f$). It may be noted that the streamwise extent of the vorticity that has issued out of the leaflets is about $x/L_f \approx 2$ for all three cases. Hence, even though the vorticity distribution looks largely different, using flap length as a length scale for the streamwise direction indicates similarities across flap lengths.

A quantity of interest in the present experiments is the position of the generated vortices ($x_c/d$) as a function of time. The position ($x_c/d$), at a given instant, is determined by the location of the maximum centreline $u$ velocity at that time, as discussed previously in the rigid exit case, where $x_c$ for the leaflet cases is measured from the flap tip. This method of identifying the vortex location, especially in the cases with longer flaps in which the vorticity is highly distributed, works reasonably well. This can be seen, for example, in figure 21(*c*), where a dotted vertical line marks the $x$ location of the peak in centreline velocity. An evaluation of the vortex centre for this case by taking a weighted mean of the vorticity is marked by circled dots in figure 21(*c*). These weighted mean dots for positive and negative signs of vorticity fall approximately near the vertical line, thus indicating that the peak in centreline velocity is a reasonable estimator in tracking the location of the vortices with time. The vortex position ($x_c/d$) is plotted against the fluid slug length ($L/d$) for both the rigid and the leaflet cases in figure 22, for impulsively started piston motions. Here we use $L/d$ as

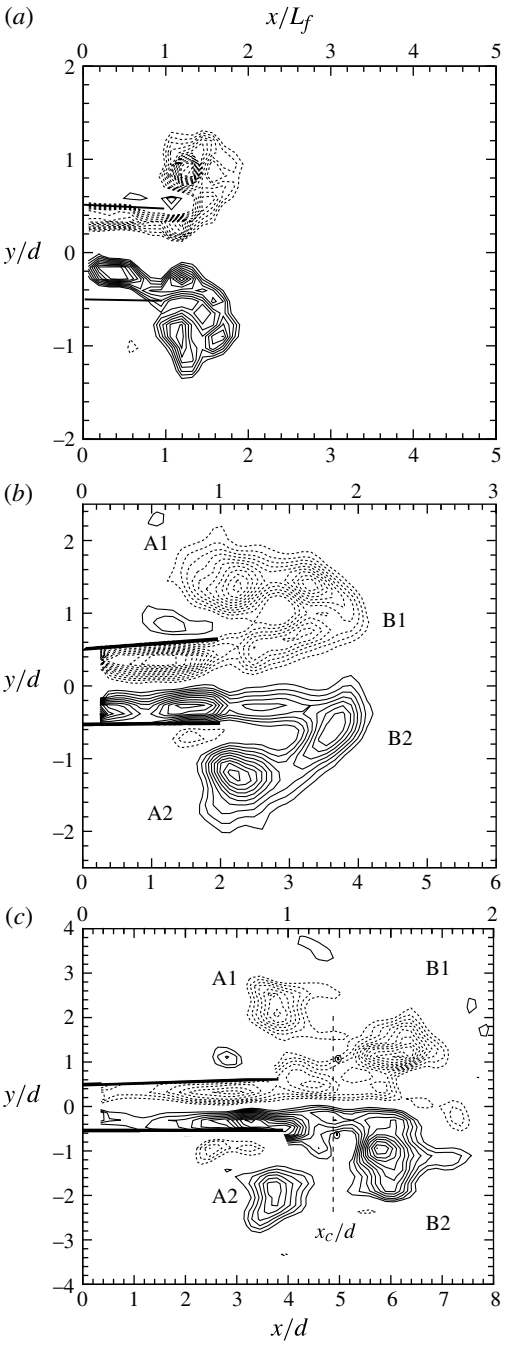


FIGURE 21. Vorticity plots for exit with hinged leaflets, with different flap lengths and an impulsively started piston motion: (*a*) $L_f/d = 1$; (*b*) $L_f/d = 2$; (*c*) $L_f/d = 4$. All the plots are at $L/L_f \approx 3.75$. The solid and dashed lines in the contours represent opposite signs of vorticity.

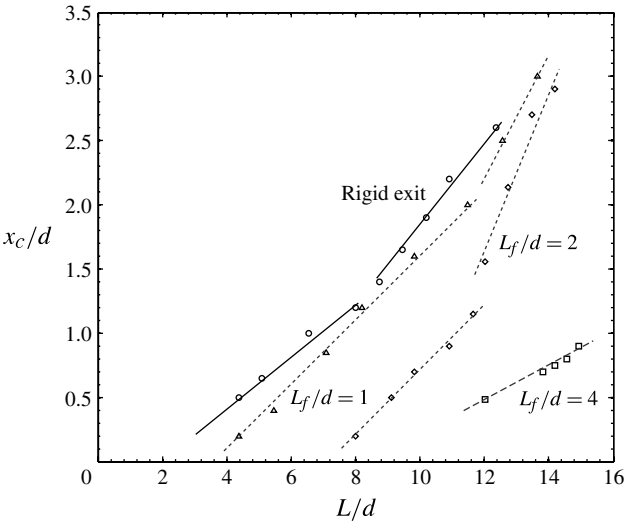


FIGURE 22. Normalized vortex centre position ($x_c/d$) as a function of fluid slug length ($L/d$), for rigid exit and exit with hinged leaflets. The piston velocity program is impulsively started for all the cases, with a maximum fluid slug length ($L/d$) of 15 in each case. The solid lines are trend lines drawn for clarity.

a time scale instead of $L/L_f$, in order to compare the flap cases with the rigid exit case ($L_f/d = 0$). The rigid exit data, as discussed earlier, shows a change in slope at a slug length ($L/d$) of approximately 9, corresponding to the emergence of a trailing jet and the detachment of the vortex from the exit, for an impulsively started piston motion. The small leaflet case with $L_f/d = 1$ shows essentially the same variation, with the data very closely following the rigid exit case. However, a change in slope for this case occurs only at $L/d = 12$. The $L_f/d = 2$ data is also initially linear with nearly the same slope as the earlier cases, and deviates from the initial linear variation again at $(L/d) \approx 12$. A difference in this case is the behaviour after $(L/d) \approx 12$, where the slope change is higher than for the rigid case and is similar to the $L_f/d = 1$ case. For $L_f/d = 4$, the fluid slug length is not large enough to see beyond the initial linear variation. Also, the slope of the curve is smaller when compared to the previous cases, suggesting that the vortices move more slowly than the previous cases. One can clearly note from the plot that with an increase in flap length, the formation of vortices is delayed, and the rate at which the vortices traverse changes with flap length.

The circulation which comes out of the rigid exit, and exit with leaflets for an impulsively started piston motion is plotted in figure 23. For the case with leaflets, circulation is measured by taking a closed contour around the vorticity outside the flap region on one side of the centreline. This is done for both sides and the absolute values are averaged to get the ejected circulation.

The measured circulation in such flows is usually normalized using a slug model prediction of the circulation. In the present case, we can find two different ways of normalizing the circulation. The first way is to use a rigid exit slug model, which is written in the standard form $\partial\Gamma/\partial t = U_p^2/2$ for an impulsively started piston motion. This model does not take into account the changes in exit opening, and is purely based on the piston velocity. Another way to normalize the circulation would be to use the slug model, but using the instantaneous exit velocity $U_e$, instead of the piston

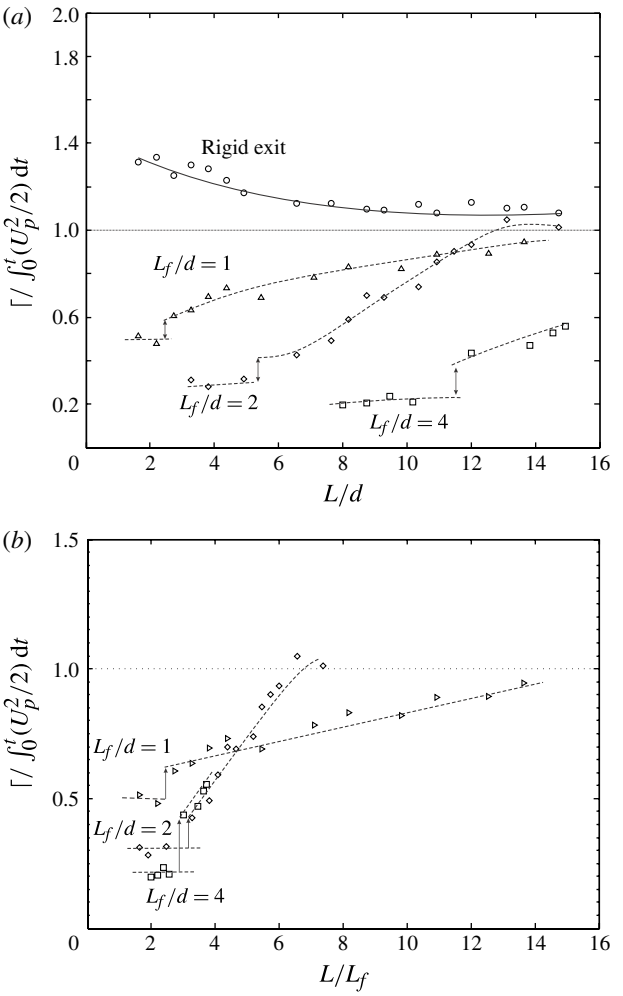


FIGURE 23. Plot of net circulation normalized with slug model for (*a*) rigid exit and leaflet cases with the time scale $L/d$, and (*b*) leaflet cases with the time scale $L/L_f$. The solid lines are trend lines drawn for clarity.

velocity $U_p$. However, $U_e$ is not known *a priori* in our experiments, and hence we use the rigid exit slug model to normalize the circulation even for the leaflet cases.

We present in figure 23(*a*) the total ejected normalized circulation as a function of $L/d$. For the rigid exit case, the measured circulation is higher than the slug model prediction. This phenomenon has been well observed for vortex rings, as first noted by Didden (1979). The observed under-prediction by the slug model, especially at the initial times, has been related to the effects of flow initiation (see Krueger 2005 for a comprehensive discussion), which is believed to be responsible for distorting the exit velocity profile, and thereby resulting in a $v$ component of velocity which contributes significantly to the circulation. This, however, is not captured in the slug model as it assumes a parallel flow at the nozzle exit. The measured circulation for the cases with leaflets is also shown in figure 23(*a*). In these cases, the net circulation coming out of the exit is significantly lower than the rigid exit case, especially at initial times.

There could be two reasons for this phenomenon. One simple reason could be that the vorticity from the separation at the hinge has not yet had time to convect out of the flaps, since the circulation values measured are only external to the flaps. The other possible reason would correspond to the case when there is no hinge separation, the vorticity in this case being formed at the flap tip where the velocities are lower (from continuity). However, once the flow develops further and the flaps stop moving, one would expect better predictions from the slug model. This is seen in figure 23(*a*) for shorter flap lengths. However, for $L_f/d = 4$, as mentioned earlier, the flaps return just before the piston stops moving, and are thus moving continuously in the duration plotted. For the longer flap this means that a lot of vorticity generated during piston motion due to separation at the hinge is still inside the flap region, which we are not measuring. We notice a jump in circulation for all three leaflet cases (at $L/d = 2.5$ for $L_f/d = 1$, at $L/d = 5.5$ for $L_f/d = 2$, and at $L/d = 11.5$ for $L_f/d = 4$). This jump could be explained by the separated vortex pair at the hinge (vortex pair B), which comes out of the flap region at around these $L/d$ values and adds on to the ejected circulation outside the flap region. This is also seen, for example, in the vorticity contour plot of figure 20. In the $L_f/d = 4$ case, even though the separated vortex pair comes out and results in a jump in circulation, the times are not large enough to permit all the vorticity from issuing out of the flap region, and hence the low values of ejected circulation at the time of piston stoppage. In figure 23(*b*) we present the same normalized circulation data as in (*a*), but plotted versus $L/L_f$ for the leaflet cases. This plot shows that the time at which the jump in circulation occurs for all three cases is close to $L/L_f \approx 3$, which is slightly before the flaps return to their initial position. The general trend of the $L_f/d = 4$ case, in particular, compares well with the $L_f/d = 2$ case in this plot. This indicates that the total circulation values for the $L_f/d = 4$ case are lower only because there has been insufficient time for the vorticity to issue out of the flaps.

## 5. Conclusions

We experimentally study the effect of having hinged leaflets at the jet exit on the formation of a two-dimensional counter-rotating vortex pair. A piston–cylinder mechanism is used to generate a starting jet from a high-aspect-ratio channel into a quiescent medium. For a rigid exit, with no leaflets at the channel exit, the measurements at a central plane show many differences with the more well-studied case of an axisymmetric vortex ring. In the present case, the vortex pair detaches from the exit and a trailing jet is seen at a much larger fluid slug length (non-dimensional piston stroke length, $L/d$) of 9, compared to the corresponding value of about 4 for the axisymmetric vortex ring. Further, the trailing jet in the present case is never detached from the vortex pair, and keeps feeding into the latter, unlike in the axisymmetric case. After the onset of a trailing jet the vortex pair translates faster, and these results are in agreement with the observations made by Afanasyev (2006), who studied two-dimensional vortex pairs experimentally. The piston velocity program is also found to change the motion of the generated vortices. Vortices generated using accelerating piston velocity programs are found to move smaller streamwise distances when compared to impulsively started velocity programs for the same ejected fluid slug length ($L/d$).

Passive flexibility is introduced in the form of rigid leaflets or flaps that are hinged at the exit of the channel, with the flaps initially parallel to the channel walls. The hinge, flap material and fluid medium (water) are chosen to closely approximate

the limiting case of a free-to-rotate rigid flap with negligible structural stiffness ($k$), structural damping ($c$) and flap inertia ($I_f$), as these limiting structural properties permit the largest flap openings. Thus, the only new parameter relevant to the flap is $L_f/d$ and perhaps represents the simplest or idealized configuration for studying interaction of unsteady flows and passive flaps. Using this arrangement, we start the flow and measure the flap kinematics and the vorticity dynamics for different flap lengths. We mainly use an impulsively started piston motion to generate the flow, which means that the piston is started impulsively from rest to a particular velocity (that is, a very large acceleration) and this velocity is maintained until the piston is brought to rest impulsively. However, we do present some results from an accelerating piston velocity program as well. The typical motion of the flaps involves a rapid opening and a subsequent more gradual return towards its initial position, after which it asymptotes to a slightly closed configuration, all while the piston is still moving.

The initial opening of the flaps can be attributed to an excess pressure that develops in the channel when the flow starts, due to the acceleration that has to be imparted to the fluid slug between the flaps. At small times, the flow around the flaps will be nearly potential in nature, and the moments acting on the flaps will be predominantly due to the excess pressure arising from the unsteady term in the Bernoulli equation and the added moment associated with the flap geometry. This was used to model the tip velocity of the flaps at flow initiation, and we find good agreement with the experimentally measured values. When the piston is impulsively stopped, the flaps close rapidly due to a low pressure developed in the channel, and can be looked at as the opposite of the over-pressure effect. The closing of the flaps while the piston is still in motion may be explained by the velocity gradient between the hinge point and the flap exit. As the flaps open, from continuity we know that the velocity at the hinge point would be larger than at the exit. This would result in lower pressure at the hinge point compared to that at the exit. This would in turn result in an inward moment on the flaps about the hinge. In reality, however, the flow is more complex, with separation and formation of various types of vortices that would definitely affect the pressures on the flaps. Using the time scale ($L/d$), the instant when the flaps reach maximum opening and the instant when they return to their initial position vary greatly with flap length. We define a new time scale based on the flap length ($L/L_f$) for the leaflet cases, and with this time scale we find that the time when the flaps reach maximum opening ($L/L_f \sim 1.75$) and when they return to their initial position ($L/L_f \sim 3.75$) is found to be nearly the same for all the impulsive velocity program cases studied, irrespective of the piston velocity and the flap length. This new time scale ($L/L_f$) comes from using the piston velocity ($U_p$) as the velocity scale and the flap length ($L_f$) as the length scale, and physically corresponds to the distance traversed by the fluid slug ($L$) compared to the flap length ($L_f$). The maximum opening angle in all these impulsive velocity program cases, irrespective of the flap length, is found to be close to 15°. In the hinged flap cases, it is found that the flap length ($L_f$) becomes the important length scale, unlike in the rigid case where it is the distance ($d$) between the rigid walls. This is also seen from PIV vorticity plots for different flap length cases, showing that the vortex structures at a given time ($L/L_f$) have traversed nearly the same number of flap lengths ($L_f$). Even though this time scale collapses the data very well for impulsively started piston motions, it does not collapse the flap motions completely when an accelerating piston motion is used.

In the case with flaps, two additional pairs of vortices are formed because of the motion of the flaps, leading to the ejection of a total of up to three vortex pairs from the hinged exit. The changes in the exit width or opening can significantly change the

distribution of the ejected vorticity, even for the same $L/L_f$. Broadly, three different kinds of vortex formation take place (figure 11). The boundary layer formed on the inner surfaces of the flaps separates at the flap tips, and a pair of counter-rotating vortices (A) are formed. Vortex pair A is analogous to the vortex pair formed in the rigid exit case. Once the flaps have opened reasonably, there is flow separation at the hinge end of the channel due to an adverse pressure gradient (similar to that in a diffuser) (figure 11*b*), and an additional vortex pair B forms. During the outward motion of the flaps, there is flow separation at the flap tips and roll-up of the boundary layer formed on the outer surfaces of the flaps, resulting in the formation of vortex pair C (figure 11*a*). Vortex pairs B and C form because of the flap motion, and are hence absent in the rigid exit case. The strength of these vortex pairs depend on the flap length and the flap motion.

In conclusion, although the flaps introduced in this work are idealized and may not represent the kind of flexibility we encounter in biological systems, it gives us a better understanding of the importance of exit flexibility in these kinds of flows.

## REFERENCES


AFANASYEV, Y. D. 2006 Formation of vortex dipoles. *Phys. Fluids* **18** (3)037103.

ANDERSON, E. J. & DEMONT, M. E. 2000 The mechanics of locomotion in the squid *Loligo pealei*: locomotory function and unsteady hydrodynamics of the jet and intramantle pressure. *J. Expl Biol.* **203**, 2851–2863.

ARAKERI, J. H., DAS, D., KROTHAPALLI, A. & LOURENCO, L. 2004 Vortex ring formation at the open end of a shock tube: a particle image velocimetry study. *Phys. Fluids* **16** (4), 1008–1019.

AUERBACH, D. 1987 Experiments on the trajectory and the circulation of the starting vortex. *J. Fluid Mech.* **183**, 185–198.

BRENNEN, C. E. 1982 A review of added mass and fluid inertial forces. *Tech. Rep.*, Department of the Navy, Port Hueneme, CA, USA.

CHENG, J. Y. & DEMONT, M. E. 1996 Hydrodynamics of scallop locomotion: unsteady fluid forces on clapping shells. *J. Fluid Mech.* **317**, 73–90.

DABIRI, J. 2009 Optimal vortex formation as a unifying principle in biological propulsion. *Annu. Rev. Fluid Mech.* **41**, 17–33.

DABIRI, J. O., COLIN, S. P. & COSTELLO, J. H. 2006 Fast-swimming hydromedusae exploit velar kinematics to form an optimal vortex wake. *J. Expl Biol.* **209** (11), 2025–2033.

DABIRI, J. & GHARIB, M. 2005*a* The role of optimal vortex formation in biological fluid transport. *Proc. R. Soc.* B **272**, 1557–1560.

DABIRI, J. O. & GHARIB, M. 2005*b* Starting flow through nozzles with temporally variable exit diameter. *J. Fluid Mech.* **538**, 111–136.

DABIRI, J. O., GHARIB, M., COLIN, S. P. & COSTELLO, J. H. 2005 Vortex motion in the ocean: *in situ* visualization of jellyfish swimming and feeding flows. *Phys. Fluids* **17** (9)091108.

DASI, L. P., GE, L., SIMON, H. A., SOTIROPOULOS, F. & YOGANATHAN, A. P. 2007 Vorticity dynamics of a bileaflet mechanical heart valve in an axisymmetric aorta. *Phys. Fluids* **19** (6)067105.

DIDDEN, N. 1979 Formation of vortex rings: rolling-up and production of circulation. *Z. Angew. Math. Phys.* **30**, 101–116.

DOMENICHINI, F., PEDRIZZETTI, G. & BACCANI, B. 2005 Three-dimensional filling flow into a model left ventricle. *J. Fluid Mech.* **539**, 179–198.

GHARIB, M., RAMBOD, E., KHERADVAR, A., SAHN, D. J. & DABIRI, J. O. 2006 Optimal vortex formation as an index of cardiac health. *Proc. Natl Acad. Sci. USA* **103**, 6305–6308.

GHARIB, M., RAMBOD, E. & SHARIFF, K. 1998 A universal time scale for vortex ring formation. *J. Fluid Mech.* **360**, 121–140.

GLEZER, A. 1988 The formation of vortex rings. *Phys. Fluids* **31**, 3532–3542.

GOVARDHAN, R. N. & WILLIAMSON, C. H. K. 2000 Modes of vortex formation and frequency response of a freely vibrating cylinder. *J. Fluid Mech.* **420**, 85–130.

KIM, D. W. Y., WALKER, P. G., PEDERSEN, E. M., POULSEN, J. K., OYRE, S., HOULIND, K. & YOGANATHAN, A. P. 1995 Left ventricular blood flow patterns in normal subjects: a quantitative analysis by three-dimensional magnetic resonance velocity mapping. *J. Am. College of Cardiology* **26**, 224–238.

KRUEGER, P. 2005 An over-pressure correction to the slug model for vortex ring circulation. *J. Fluid Mech.* **545**, 427–443.

KRUEGER, P. S. & GHARIB, M. 2003 The significance of vortex ring formation to the impulse and thrust of a starting jet. *Phys. Fluids* **15**, 1271–1281.

LEE, C. S. F & TALBOT, L. 1979 A fluid-mechanical study of the closure of heart valves. *J. Fluid Mech.* **91**, 41–63.

LIM, T. T. & NICKELS, T. B. 1995 Vortex rings. In *Fluid Vortices*, pp. 95–153. Kluwer.

LINDEN, P. F. & TURNER, J. S. 2004 'Optimal' vortex rings and aquatic propulsion mechanisms. *Proc. R. Soc. Lond.* B **271** (1539), 647–653.

LISOSKI, D. L. A. 1993 Nominally two-dimensional flow about a normal flat plate. PhD thesis, California Institute of Technology.

MAXWORTHY, T. 1972 The structure and stability of vortex rings. *J. Fluid Mech.* **51**, 15–32.

MAXWORTHY, T. 1974 Turbulent vortex rings. *J. Fluid Mech.* **64**, 227–239.

MAXWORTHY, T. 1977 Some experimental studies of vortex rings. *J. Fluid Mech.* **81**, 465–495.

MOHSENI, K., RAN, H. & COLONIUS, T. 2001 Numerical experiments on vortex ring formation. *J. Fluid Mech.* **430**, 267–282.

PEDRIZZETTI, G. 2010 Vortex formation out of two-dimensional orifices. *J. Fluid Mech.* **655**, 198–216.

PEDRIZZETTI, G. & DOMENICHINI, F. 2006 Flow-driven opening of a valvular leaflet. *J. Fluid Mech.* **569**, 321–330.

PEDRIZZETTI, G. & DOMENICHINI, F. 2007 Asymmetric opening of a simple bileaflet valve. *Phys. Rev. Lett.* **98**, 214503.

RINGUETTE, M. J., MILANO, M. & GHARIB, M. 2007 Role of the tip vortex in the force generation of low-aspect-ratio normal flat plates. *J. Fluid Mech.* **581**, 453–468.

ROMANO, G. P., QUERZOLI, G. & FALCHI, M. 2009 Investigation of vortex dynamics downstream of moving leaflets using robust image velocimetry. *Exp. Fluids* **47**, 827–838.

ROSENFELD, M., RAMBOD, E. & GHARIB, M. 1998 Circulation and formation number of laminar vortex rings. *J. Fluid Mech.* **376**, 297–318.

SHARIFF, K. & LEONARD, A. 1992 Vortex rings. *Annu. Rev. Fluid Mech.* **24**, 235–279.

SHUSSER, M. & GHARIB, M. 2000 Energy and velocity of a forming vortex ring. *Phys. Fluids* **12** (3), 618–621.

SHUSSER, M., ROSENFELD, M., DABIRI, J. O. & GHARIB, M. 2006 Effect of time-dependent piston velocity program on vortex ring formation in a piston/cylinder arrangement. *Phys. Fluids* **18** (3)033601.

YOGANATHAN, A. P., HE, Z. & JONES, S. C. 2004 Fluid mechanics of heart valves. *Annu. Rev. Biomed. Engng* **6**, 331–362.